Key Points:
- Intrinsic orogenic processes during the construction of the central Andes govern the stress field evolution
- Paleostress analysis allows us to identify two geodynamic stages: the Altiplano/Puna plateau construction and its gravitational collapse
- The tectonic regime varied from compression to strike slip to extension, with transitions due to principal stress axis permutations

Supporting Information:
- Supporting Information S1

Correspondence to:
L. Giambiagi,
lgiambiagi@mendoza-conicet.gob.ar

Temporal variation of the stress field during the construction of the central Andes: Constrains from the volcanic arc region (22–26°S), Western Cordillera, Chile, during the last 20 Ma

Laura Giambiagi[1], Pamela Alvarez[2], and Silvana Spagnotto[3]

[1]IANIGLA, CCT Mendoza, CONICET, Mendoza, Argentina, [2]TEHEMA, Pirque, Chile, [3]CONICET–Departamento de Física, Universidad Nacional de San Luis, San Luis, Argentina

Abstract In order to understand the response of the stress field state to intrinsic processes during the construction of the Andes, such as thickening of the continental crust, lithospheric delamination, and/or thermal weakening, we investigate the stress field evolution of the arc region since the last 20 Myr, in the central Andes (22–26.5°S). The 43 reduced paleostress tensors derived from inversion of 682 fault slip data reveal a complex pattern of stress states during the last episode of orogenic construction and topographic uplift. We identify two geodynamic stages: the first stage corresponds to the construction of the Altiplano/Puna plateau and the second one to its gravitational collapse. Four stress states that have prevailed in the Altiplano/Puna plateau since middle Miocene times characterize the transition from one stage to the other. Along the study latitudes, a spatiotemporal change in stress state is clearly observed, which led to an understanding that a change in the stress field may be related not only to the boundary conditions but also to intrinsic factors associated with the construction of the Andean orogeny. Our results suggest that approximately at 13–10 Ma and approximately 8–5 Ma, in the southern Altiplano and northern Puna, and in the southern Puna, respectively, regional elevation and crustal thicknesses reached threshold values necessary to generate the orogenic collapse.

1. Introduction

Deciphering the state of stress within the central Andes and its spatiotemporal evolution through the last episode of orogenic construction can place crucial constraints on the dynamics of plate convergence and mechanical behavior of the upper plate. The formation of mountains and crustal roots by driving plate tectonic forces is associated with an increase gravitational potential energy [*Artyushkov*, 1973]. As a result, for specific driving forces, both the mean height of the range and the thickness of the crust should reach a limiting value [*Molnar and Tapponnier*, 1978]. When this value is achieved, the mountain range is likely to grow laterally in width instead of increasing in height [*Molnar and Lyon-Caen*, 1988; *Hoke et al.*, 2014; *Giambiagi et al.*, 2015]. Topographic uplift is the result of crustal shortening and generation of a crustal root, but variations in the rheology and thermal structure of the lithosphere, by processes such as lithospheric thinning, have important effects on deformation and topography [*Houseman et al.*, 1981; *Isacks*, 1988].

Several studies from the High Andes of Perú and Bolivia have revealed the existence of a Quaternary extensional regime with SH_{min} oriented parallel to the strike of the Andes (Figure 1a) [*Heidbach et al.*, 2008b, and references therein], presumably as a consequence of excess of gravitational potential energy due to the ~4000 m high topographic elevation [*Dalmayrac and Molnar*, 1981; *Mercier*, 1981; *Sébrier et al.*, 1985, 1988b; *Mercier et al.*, 1992; *Assumpção and Araujo*, 1993]. In the Altiplano/Puna plateau, previous structural studies reveal important kinematic changes during the late Cenozoic deformation from contraction to extension [*Allmendinger et al.*, 1989; *Marrett et al.*, 1994; *Cladouhus et al.*, 1994; *Riller et al.*, 2001; *Elger et al.*, 2005; *Tibaldi et al.*, 2009; *Acocella et al.*, 2011; *Lanza et al.*, 2013; *Daxberger and Riller*, 2015]. These studies suggest that, despite ongoing overall shortening in the Andean orogen, the gravitational stresses initiate normal and strike-slip faulting and force deformation toward lower elevations in the foreland.

Whereas extensional and compressional stress regimes at the High Andes have been explained by a combination of tectonic and buoyancy forces, as the crust gets thick and isostasy produces topographic uplift [*Fleitout and Froidevaux*, 1982; *Froidevaux and Isacks*, 1984; *Molnar and Lyon-Caen*, 1988; *Richardson and Coblentz*, 1994], uncertainties remain regarding the precise temporal patterns of stress field states and the way the transition from compression to extension occurred. In the Andes of central Perú, the model proposed
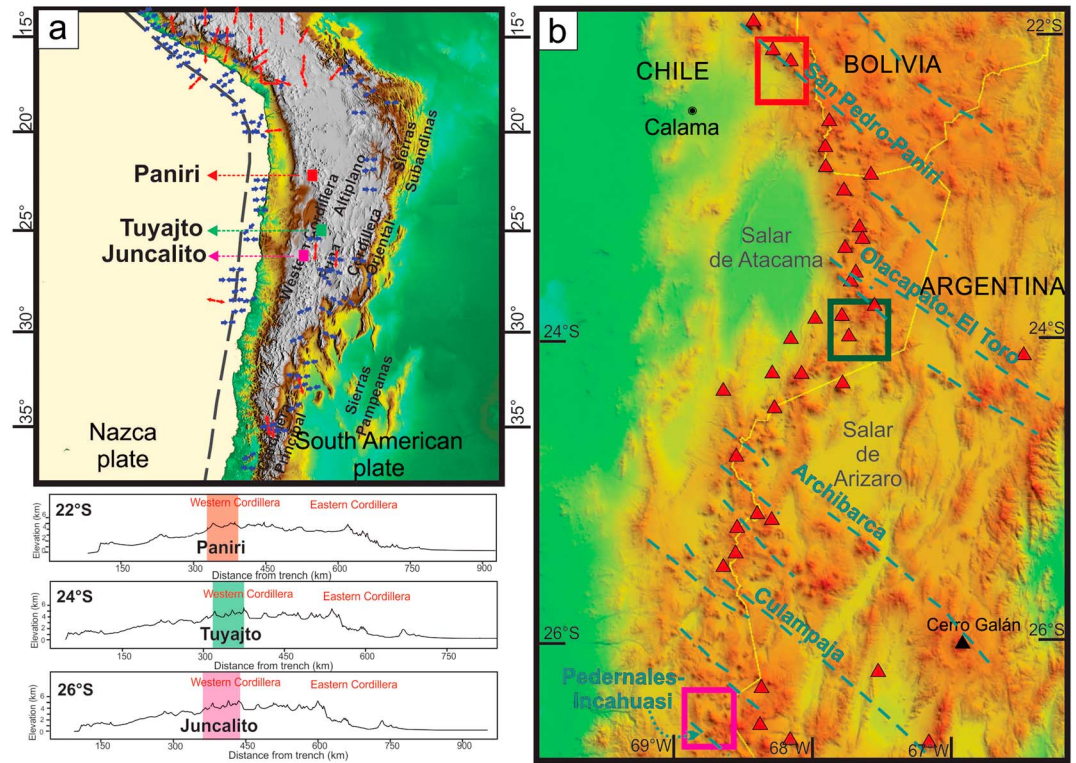
Figure 1. (a) Regional shaded relief map of the central Andes and topographic profiles at 22, 24, and 26.5°S. The study areas are located at the southern Altiplano, northern Puna, and southern Puna latitudes, respectively. The red and blue arrows represent the extension and compression axes, respectively, obtained from the World Stress Project (http://dc-app3-14.gfz-potsdam.de/). (b) Detail shaded relief map with location of the three study areas along the Western Cordillera, in Chile, showing the distribution of volcanoes and main NW lineaments.

by *Sébrier et al.* [1988b] indicates that at a mean elevation higher than 4000 m, and lower than 3700 m, extensional and compressional stress fields dominate, respectively. Between 3700 and 4000 m of mean elevation, these authors proposed a transitional state of stress dominated by compressional/strike-slip tectonics, when σ_{zz} changes from σ_3 to σ_2.

Heidbach et al. [2008a] suggest that the tectonic regime in the central Andes changed significantly during the last 10 Ma, due to response to the Andean topography growth. Nevertheless, the available data do not provide a complete record of this temporal pattern. The purpose of this study is threefold: (1) document temporal changes in stress fields at the backbone of the Andes during the construction of the Altiplano/Puna plateau, (2) understand how the change from compression to extension occurred, and (3) discuss possible mechanisms which may account for the observed stress field evolution. We present new kinematic data recollected throughout the middle Miocene to Present arc region (Figure 1b) and establish stress field patterns. We identify two geodynamic phases, the first one corresponding to the construction of the plateau and the second one to its gravitational collapse. We explore the potential of using changes in stress field patterns as an indicator for changes in the topographic elevation and/or boundary conditions over time.

2. Regional Setting

The central Andes results from the convergence between the Nazca and South American plates at approximately 80 mm/a in an ENE direction (NUVEL-1A) [*DeMets et al.*, 1994]. The reduction of approximately 30% in convergence rate in the last 10 Ma, from 10.3 ± 0.2 cm/a [*Gordon and Jurdy*, 1986] to 6.7 ± 0.2 cm/a [*Sella et al.*, 2002], occurred synchronously with an increasing shortening rate at the Altiplano latitudes (~18–23°S) from ~5–8 mm/a to ~10–15 mm/a [*Hindle et al.*, 2002]. Numerical models that couple global mantle circulation with lithospheric dynamics assign this reduction to the growth of the Andean mountain [*Iaffaldano et al.,*

2006; *Heidbach et al.*, 2008a]. This suggests that an important increase in crustal shortening may have occurred between 10 and 6 Ma in accordance with ductile lower crustal flow and underthrusting of the South American craton below the Andean strip [*Allmendinger and Gubbels*, 1996; *Barke and Lamb*, 2006].

The study areas lie in the Western Cordillera (Figure 1a), representing the western margin of the Altiplano/Puna plateau, along the volcanic arc (Figure 1b). The high topography of this area is sustained by a 65 to 75 km thick crust [*Beck and Zandt*, 2002; *McGlashan et al.*, 2008] and a thermally thinned lithosphere underlain by low-density asthenosphere [*Froidevaux and Isacks*, 1984].

One of the main morphostructural patterns in the arc region is formed by NW trending structural and magmatic lineaments crosscutting the Altiplano/Puna plateau [*Allmendinger et al.*, 1983; *Salfity*, 1985; *Riller et al.*, 2001; *Chernicoff et al.*, 2002; *Matteini et al.*, 2002; *Petrinovic et al.*, 2006; *Acocella et al.*, 2011], such as the Olacapato-El Toro, Archibarca, and Culampaja lineaments (Figure 1b). These lineaments can be traced into the Western Cordillera, where they apparently died out. In detail, they are characterized by subparallel regional faults with Plio-Quaternary sinistral strike-slip movement and associated volcano feeding systems [*Marrett et al.*, 1994; *Riller et al.*, 2001; *Acocella et al.*, 2011; *Bonali et al.*, 2012; *Lanza et al.*, 2013].

3. Methods

We examine three areas across the late Cenozoic volcanic arc (Figure 1): Paniri (22°S), Tuyajto (24°S), and Juncalito (26.5°S). The structural study comprises recognition during field survey of major faults and previously described lineaments, the construction of structural cross sections, kinematic analysis of major and mesoscale faults, and paleostress inversion of fault slip data to reconstruct the areal and temporal distributions of reduced stress tensors. The kinematic/dynamic analysis consisted on the measurement of fault plane-striation data at (i) the main fault planes and their subsidiary fault planes for the kinematic analysis and (ii) mesoscale faults measured at stations distributed all along the study areas to obtain reduced stress tensors. Our data set consists of more than 1000 fault slip data, one third of which were used for the kinematic analysis (see Kinematic analysis in the supporting information). We have focused on data with reliable shear indicators, mainly striations with associated fractures and mineral growth fibers. Because this research focused on Miocene-Quaternary stress regimes, localities with rocks older than Miocene were not considered due to the possible presence of faults related to previous deformational events.

With this methodology, we were able to determine the different deformational events that affect the study areas and assign a relative time for each. After we were confident with the kinematic analysis, we selected the measurement sites to reconstruct the paleostresses, providing the age of the rocks was known. Data set for the paleostress reconstructions consist of 682 measurements of slip data from mesoscale fault collected at 38 stations (Table 1).

We paid particular attention to the separation of homogeneous fault sets from heterogeneous population. The procedure for separating superimposed stress tensors relies first on relative tectonic chronology data and then on both mechanical and kinematic compatibilities. First, we analyzed kinematic data of the youngest rocks, which are Pleistocene-Holocene volcanic rocks. Ages of the volcanic rocks allow us to estimate the maximum age of brittle deformation for each location. We used these data and compatibility criteria to separate heterogeneous data into homogeneous subsets for Pliocene rocks first and Miocene rocks second. After this rough separation, the final separation of the data was obtained mathematically by eliminating data with large angles between measured and theoretical slip directions.

We perform a paleostress inversion and obtain paleostress axis and stress ratios, which provide a dynamic interpretation of the kinematic analysis previously done (Table S2 in the supporting information). To perform the inversion we applied the multiple-slip method implemented in the T-TECTO 3.0 program [*Zalohar and Vrabec*, 2007] and obtained 43 reduced paleostress tensors (axes of σ_1, σ_2, and σ_3 and stress ratio ϕ) for the Miocene-Quaternary capable of explaining the direction of slip on most of the measured mesoscale faults. The stress ratio ϕ constrains the shape of the ellipsoid $\phi = (\sigma_2 - \sigma_3)/(\sigma_1 - \sigma_3)$ and together with the orientation of the principal stress axes define the reduced stress tensor. The relative magnitudes of principal stresses vary between three end-member tectonic regimes with reference to the vertical principal stress S_v: compressional ($S_v = \sigma_3$), strike-slip ($S_v = \sigma_2$), and extensional ($S_v = \sigma_1$) regimes. Inside these three end-member major types, the stress regime also varies as a function of the stress radio ϕ. We used the stress index R' proposed by

Table 1. Trend and Plunge of Each Principal Stress Axis (σ_1, σ_2, and σ_3), ϕ Ratio, and α Misfit Angle[a]

						Paniri (22°S)							
Site	Latitude S	Longitude W	n	nT	σ_1	σ_2	σ_3	ϕ	α	Q	R'	Regime	Timing
101	22°25′04″	68°09′24″	10	10	003/75	201/14	110/4	0.2	13°	B	0.2	E'	>6.52 (Toconce Ignimbrite)
102	22°23′36″	68°08′01″	18	21	002/86	213/3	122/2	0.3	21°	B	0.3	E	<4.5 (Puripicar Ignimbrite)
103	22°25′19″	68°09′37″	19	23	300/75	187/6	96/13	0.1	25°	C	0.1	E'	>6.52 (Toconce Ignimbrite)
104a	22°20′59″	68°17′29″	14	14	151/75	026/8	295/12	0.2	22°	B	0.2	E'	<8.8 (Sifón Ignimbrite)
104b	22°20′59″	68°17′29″	32	32	002/23	167/66	270/6	0.6	21°	A	1.4	SL	<8.8 (Sifón Ignimbrite)
105	22°21′07″	68°18′57″	15	15	101/2	197/72	010/18	0.2	16°	B	1.2	SL/C	<8.8 (Sifón Ignimbrite)
106a	22°20′03″	68°17′39″	27	27	002/86	189/4	98/0	0.1	20°	B	0.1	E'	<8.8 (Sifón Ignimbrite)
106b	22°20′03″	68°17′39″	14	14	346/2	77/24	252/66	0.0	26°	B	2	SL/C	<8.8 (Sifón Ignimbrite)
107	22°20′06″	68°17′55″	23	24	346/2	82/72	255/18	0.0	20°	B	2	SL/C	>8.8 (Sifón Ignimbrite)
108	22°18′49″	68°17′25″	18	20	193/0	101/85	283/5	0.1	22°	B	1.9	SL/C	<10.18 (Divisoco Ignimbrite)
109	22°18′49″	68°17′25″	14	15	076/2	166/2	301/87	0.8	22°	B	2.8	C'	>10.18 (Divisoco Ignimbrite)
110	22°21′01″	68°18′50″	12	12	086/13	356/2	257/77	0.6	15°	B	2.6	C	> Pliocene (El Loa Gr)
111	22°21′01″	68°18′50″	12	12	151/76	050/3	319/14	0.0	15°	B	0	E'	<8.8 (Sifón Ignimbrite)
112	22°21′47″	68°18′50″	10	10	89/65	276/25	184/3	0.9	4°	A	0.9	SL/E	<8.8 (Sifón Ignimbrite)
113a	22°22′02″	68°16′40″	10	10	132/65	305/25	037/3	0.2	8°	B	0.2	E'	>Late Cretaceous
113b	22°22′02″	68°16′40″	19	19	156/1	251/77	65/13	1.0	14°	B	1	SL/E	>Late Cretaceous
114	22°21′56″	68°16′45″	12	12	114/13	204/2	303/77	0.6	18°	B	2.6	C	>10.18 Ma
115	22°17′59″	68°21′57″	10	10	170/12	74/23	286/63	0.1	13°	C	2.1	SL/C	<10.18 (Divisoco Ignimbrite)
Total			289	300									
						Tuyajto (24°S)							
Site	Latitude S	Longitude W	n	nT	σ_1	σ_2	σ_3	ϕ	α	Q	R'	Regime	Timing
201	23°54′37″	67°47′33″	13	13	226/76	15/13	107/7	0	20°	B	0	E'	<6.17 Ma
202	23°54′36″	67°47′38″	11	12	15/002	123/84	285/6	0.8	12°	B	1.2	SL/E	<6.17 Ma
203	23°53′58″	67°50′50″	24	24	72/12	278/76	163/6	0.8	19°	B	1.2	SL/E	<2.7 Ma Patao-Tucúcaro Ignimbrite
204	23°50′06″	67°29′34″	16	16	196/23	001/66	104/6	0.9	21°	B	1.1	SL/E	<7.7 Ma and >5.9 Ma
205	23°48′54″	67°29′18″	11	12	273/86	123/3	32/002	0.2	15°	B	0.2	E/SL	<4.8
206	23°48′06″	67°29′51″	12	12	273/86	123/3	32/2	0.0	20°	B	0	E'	<2.0
207	23°48′04″	67°29′55″	23	23	285/2	176/84	15/006	0.5	21°	B	1.5	SL	<4.4 and >2.0 Ma
208	24°02′48″	67°40′44″	15	16	58/13	212/76	327/6	0.7	19°	B	1.3	SL	<late Miocene
209	23°59′48″	67°44′49″	22	25	273/86	86/4	177/0	0.2	23°	B	0.2	E	<2.7 Ma Patao-Tucúcaro Ignimbrite
210	24°04′51″	67°50′41″	15	15	67/23	232/66	335/6	0.8	12°	B	1.2	SL/E	
211	23°51′51″	67°35′12″	10	10	002/86	189/004	98/0	0.1	8°	B	0.1	E'	Pleistocene
212	23°51′36″	67°35′48″	16	24	002/86	225/3	134/3	1.0	23°	B	1	SL/E	Pliocene-early Pleistocene
213	23°50′36″	67°27′49″	13	13	003/65	202/24	109/8	0.7	20°	C	0.7	SL	<late Miocene and >late Pliocene
Total			201	215									
						Juncalito (26.5°S)							
Site	Latitude S	Longitude W	n	nT	σ_1	σ_2	σ_3	ϕ	α	Q	R'	Regime	Timing
301	26°31′15″	68°54′16″	16	16	260/2	350/2	125/87	0.3	16°	B	2.3	C	20 > T > 13 Ma
302	26°29′40″	68°50′19″	11	11	97/12	187/2	286/78	0.7	14°	B	2.7	C	20 > T > 13 Ma
303	26°40′48″	68°50′50″	9	9	76/2	167/12	337/78	0.6	17°	B	2.6	C	20 > T > 13 Ma
304	26°16′11″	68°50′37″	12	13	348/65	80/1	170/25	0.3	14°	B	0.3	E	<Pleistocene
305	26°15′32″	68°52′33″	16	19	346/002	255/024	081/066	0.1	17°	B	2.1	SL/C	<19 Ma
306	26°32′36″	68°53′53″	18	19	88/2	340/84	179/6	0.7	24°	B	1.3	SL/E	<early Miocene
307	26°32′16″	68°47′05″	11	12	164/23	23/61	261/17	0.3	24°	C	1.7	SL/C	<3.18
308a	26°32′25″	68°45′59″	9	9	219/065	342/014	077/020	0.5	25°	C	0.5	E	<2.4
308b	26°32′25″	68°45′59″	17	18	248/2	356/84	158/6	0.8	24°	B	1.2	SL/E	<2.4
309	26°32′44″	68°46′7″	10	12	273/086	123/003	032/002	0.3	21°	C	0.3	E	<2.4
310a	26°37′20″	68°50′31″	9	10	003/65	202/24	109/8	0.2	23°	C	0.2	E'	<13.0 Ma
310b	26°37′20″	68°50′31″	35	46	271/86	74/4	165/1	0.7	23°	B	0.7	SL/E	<13.0 Ma
Total			146	167									

[a]Stress regimes: C' radial compression, C pure compression, C/SL compression/strike slip, SL/C strike slip/compression, SL pure strike slip, SL/E strike slip/exten-sion, E/SL extension/strike slip, E pure extension, and E' radial extension. nT: number of measured fault slip data, n: number of fault slip data used for the obtained paleostress tensor. Q: accuracy parameter R': stress index.

Delvaux et al. [1997] to express numerically the stress regime. In an extensional stress regime ($S_v = \sigma_1$), $R' = \phi$, and the regimes can be classified into radial extension ($0 < R' < 0.25$), pure extension ($0.25 < R' < 0.75$), and extension/strike slip ($0.75 < R' < 1$). In a strike-slip regime ($S_v = \sigma_2$), $R' = 2 - \phi$, and the regimes can be strike slip/extension ($1 < R' < 1.25$), pure strike slip ($1.25 < R' < 1.75$), and strike slip/compression ($1.75 < R' < 2$). In a

compressional regime, $R' = 2 + \phi$, and the regimes can be compression/strike slip ($2 < R' < 2.25$), pure compression ($2.25 < R' < 2.75$), and radial compression ($2.75 < R' < 3$).

Evidence concerning the relative chronology between different paleostress states allows us to propose a possible sequence of stress evolution. We implement the quality ranking proposed by *Delvaux et al.* [1997]. This quality rank depends on the number of data (n), the ratio of used data versus total collected data (n/nt), and the misfit angle (α). Accuracy parameter [$n \times (n/nt)/\alpha$] > 1.5, 0.5–1.5, 0.3–0.5, and <0.3 indicates an A, B, C, or D quality, respectively. Additionally, for the tensor results poorly constrained with not enough different fault geometries, we lower one quality rank (from A to B, etc.).

The stress inversion method is a powerful tool with successful results as long as several precautions are taken [*Lacombe*, 2012, and references therein]. In order to diminish perturbation of the local stress field by fault slip [*Kaven et al.*, 2011] we measured mesoscale faults with as much diverse orientation as possible, including a variety of fault orientations, and compared results obtained from different measurement stations, located near or far away from the principal faults. Other important caution is the existence of vertical block rotations that could affect the measured rocks. Paleomagnetic studies in the Chilean Precordillera indicate a lack of rotation about vertical axes in lower Miocene to Quaternary rocks, suggesting that clockwise rotations found in older rocks were completed before the late Cenozoic [*Somoza and Tomlinson*, 2002; *Arriagada et al.*, 2003].

We compare data obtained from sites composed of (i) several flat-lying ignimbrites and volcanic rocks, (ii) upper Miocene sedimentary sequences buried by Plio-Quaternary volcanic flows, and (iii) partially eroded Miocene-Pliocene volcanoes. The advantage of studying partially eroded volcanoes is that deep deformational processes can be examined. Moreover, the continuous record of volcanic rocks allows us to assign a timing for each identified state of stress and obtain a temporal sequence of types of tensors. Caution should be taken, on the other hand, with local stress perturbation due to magma intrusion [i.e., *Gudmundsson*, 2006]. For that reason, we compare results obtained from volcanoes and sites located away from them.

4. Results

4.1. Paniri (22°S)

The Paniri area is located close to the border between Chile and Bolivia, at the southern Altiplano latitudes (Figure 2a), where the Miocene to Present volcanic arc is aligned along the NW regional San Pedro-Paniri lineament. In this area, Permo-Triassic volcanic and Upper Cretaceous to lower Miocene sedimentary rocks are covered by flat-lying ignimbrites (Figure 2b), interbedded with lacustrine and alluvial sediments of late Miocene to early Pliocene age [*Blanco and Tomlinson*, 2009].

We identified two main thrust faults, Toconce and Cerro de Alquina, which uplift the Permo-Triassic rocks on top of the Cretaceous sedimentary rocks. These faults are unconformably covered by the Divisoco Ignimbrite (10.18 Ma [*Salisbury et al.*, 2011]), dating their activity >10 Ma. On the other hand, the Sifón Ignimbrite (8.8 Ma [*Salisbury et al.*, 2011]) is affected by the Baños del Turi conjugate system (Figure 2b) composed of NNE striking sinistral faults (faults I and II; Figure 3), with associated N triking Riedel fractures, and NNW striking dextral strike-slip faults (faults III and IV; Figure 3). These rocks are also affected by NNE to N-S trending normal and normal-sinistral faults. Crosscutting relationships indicate that normal faults postdate the strike-slip conjugate fault system, but both strike-slip and normal faults do not affect the Toconce Ignimbrite (6.52 Ma [*Salisbury et al.*, 2011]), constraining the age of strike-slip and normal faults between 8.8 and 6.52 Ma. The Divisoco faults (Figure 3b) affect the Divisoco Ignimbrite and present a dextral movement.

The Toconce Ignimbrite (6.52 Ma) is affected by another conjugate system of NE to ENE dextral and WNW sinistral faults and E-W to NNW normal faults (Figure 4). Sinistral faults, related to the San Pedro-Paniri lineament (Figure 2), were active during this event.

Throughout the region, we obtained 18 reduced paleostress tensors and classified five tectonic regimes (Figure 5): (1) a pure compression regime with E-W σ_1 (Figure 5a), constrained between the early Miocene and 10.18 Ma (Divisoco Ignimbrite); (2) a strike-slip/compression regime with N-S σ_1 (Figure 5b), younger than 10.18 Ma but older than 6.52 Ma (Toconce Ignimbrite); (3) a strike-slip/extension regime with ENE to ESE σ_3 (Figure 5c), older than 6.52 Ma (Toconce Ignimbrite) and older than the strike-slip/compression regime; (4) a pure strike-slip to extension/strike-slip regime with E-W σ_1 (Figure 5d), younger than 8.8 Ma (Sifón Ignimbrite); and (5) an extension regime (Figure 5e) younger than 4.5 Ma (Puripicar Ignimbrite
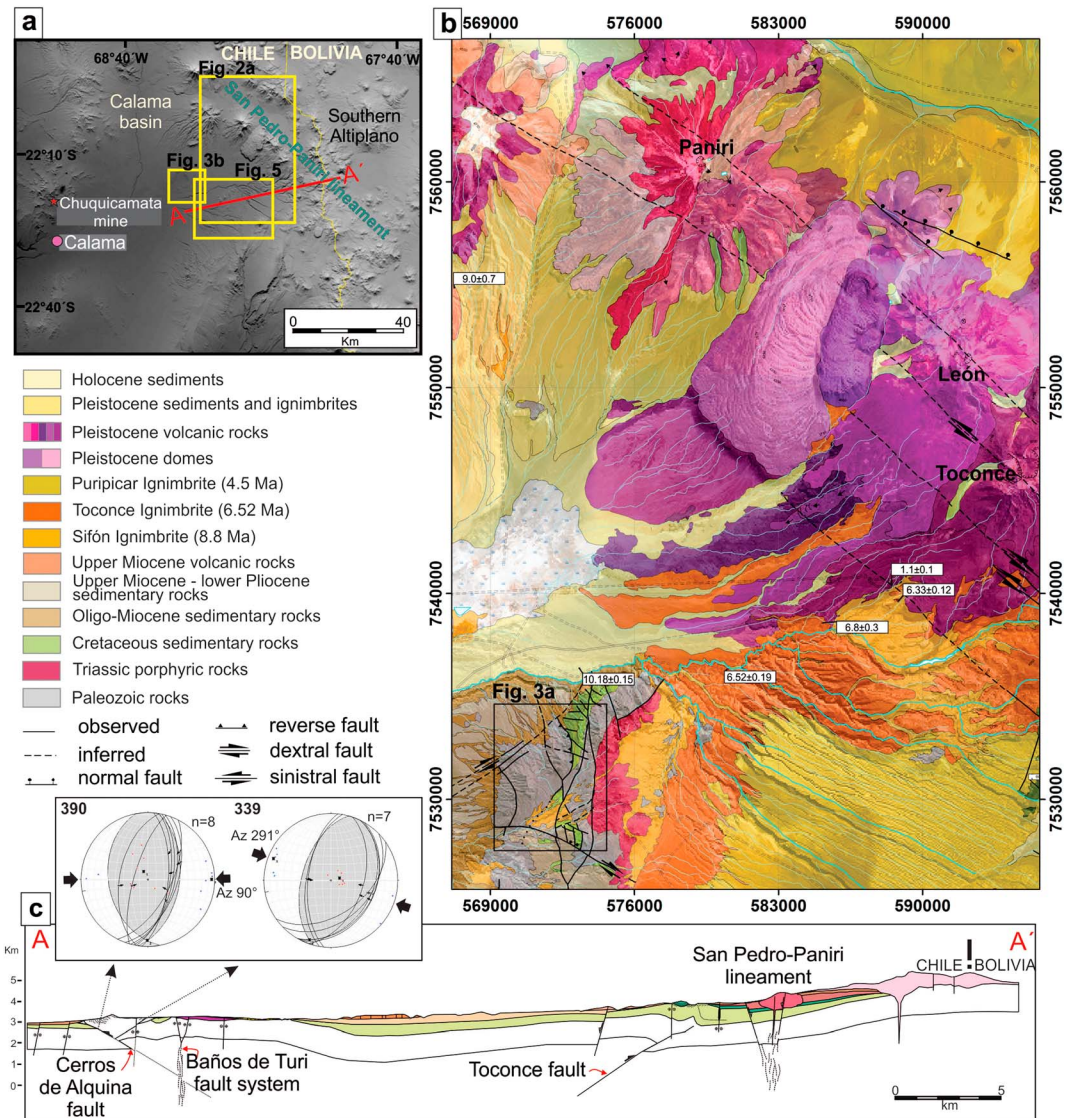
Figure 2. (a) Shaded relief map of the Paniri area and surrounding regions. (b) Topography, geology, and structure of the Paniri area, based on *Polanco et al.* [2015]. Location in Figure 2a. (c) Cross section along A-A' transect in Figure 2a, and kinematic data from Cerros de Alquina reverse fault, indicating a E-W to WNW direction of contraction. Radimetric ages from *Salisbury et al.* [2011], *Marinovic and Lahsen* [1984], and *Lahsen and Munizaga* [1979].

[*Marinovic and Lahsen*, 1984]) and still active after the Pleistocene eruption of the Paniri volcano. The Sifón ignimbrite episode (8.8 Ma) occurred during the strike-slip/compression event 2, as faults from one of these stations were unconformably covered by it, while in other stations, the ignimbrite is crosscut by the strike-slip/reverse fault system.

4.2. Tuyajto (24°S)

At 23–24°S latitudes, the late Cenozoic volcanic arc is located eastward of the Preandean depression where the Salar de Atacama basin is developed [*Mpodozis et al.*, 2005]. Altitudes at this basin, ~2300 m, contrast with altitudes (~4100 m) of the salars inside the volcanic arc (Figure 1b). In this area, the WNW dipping reverse Miscanti fault (Figure 6) uplifts the Upper Paleozoic and Cretaceous rocks over the Oligocene-lower Miocene sedimentary rocks [*González et al.*, 2009].

To the east, the Arizaro fault is an inferred reverse structure, responsible for the uplift of the Paleozoic basement rocks on top of the Oligocene-lower Miocene rocks. Three main lineaments, Capur, Cosor, and
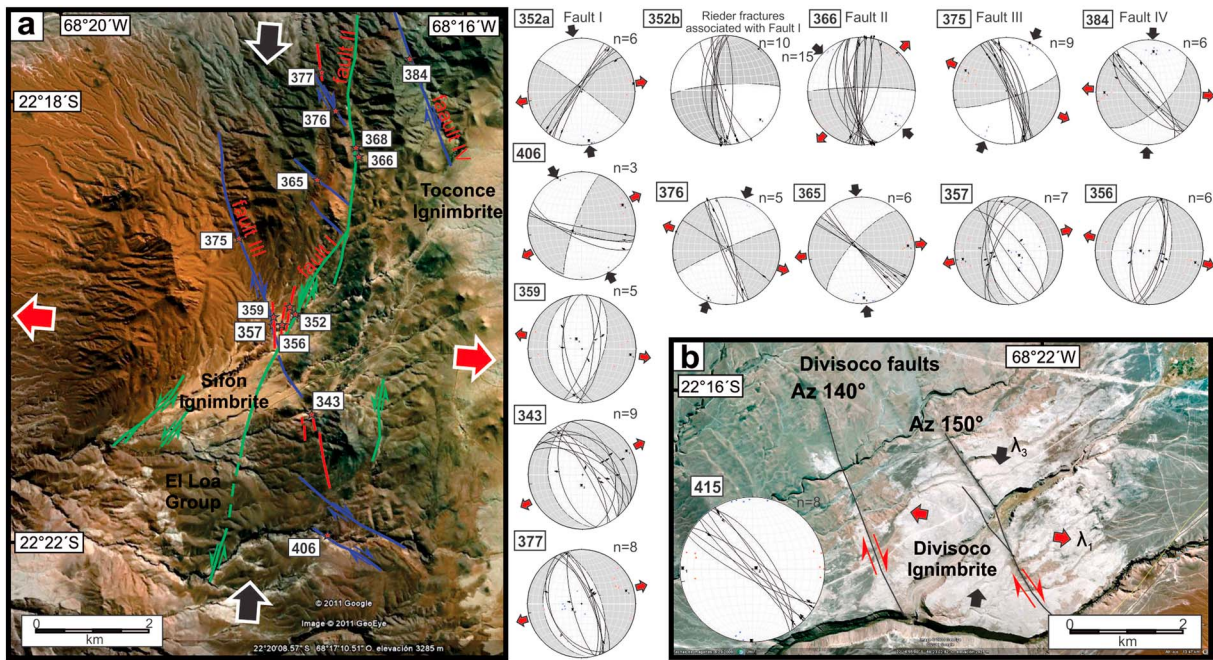
Figure 3. (a) Structural map of the southwestern sector of the Paniri area (location in Figure 2b), showing the Baños del Turi conjugate fault system, with lower hemisphere equal-area projections (using FaultKinWin® from *Allmendinger* [2001]) of orientation and sense of slip of faults. The black and red arrows indicate the contractional (λ_3) and stretching directions (λ_1), respectively. (b) Google Earth image and kinematics for the Divisoco faults. Location in Figure 2a.
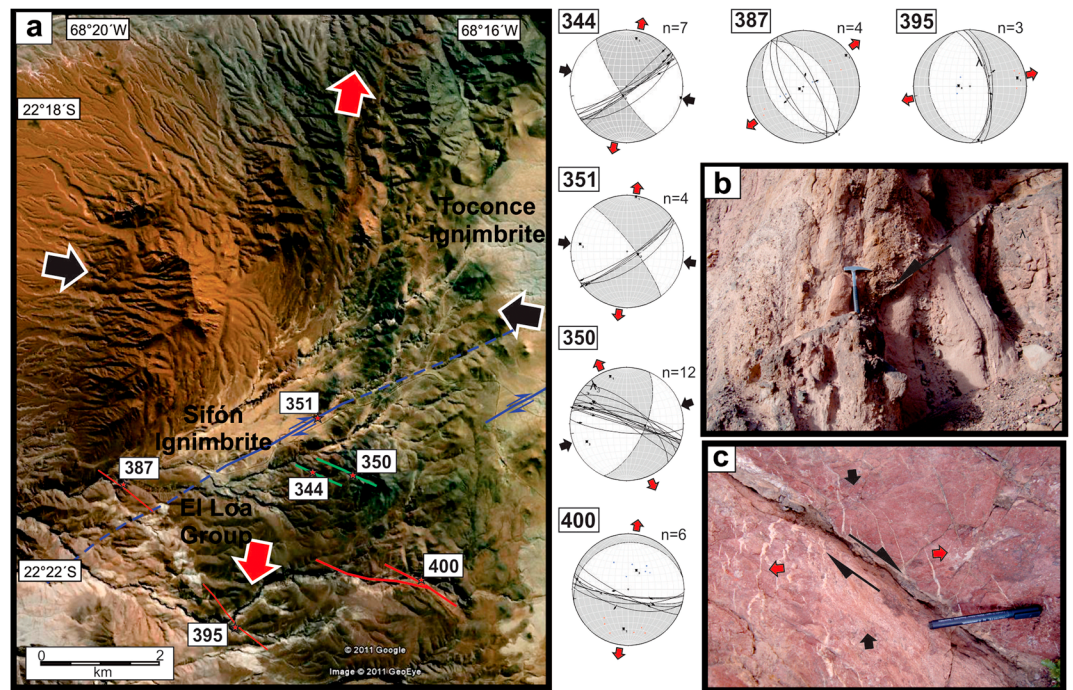
Figure 4. (a) Satellite image of the same area of Figure 3a (see location in Figure 2b), with location of kinematic stations. Data is projected into lower hemisphere equal-area stereonets using FaultKinWin®. The purple, green, and red lines are the dextral, sinistral, and normal faults, respectively. (b) Example of WNW striking normal faults affecting the El Loa sedimentary rocks at site 400. (c) View from top of a NE striking dextral strike-slip fault at site 351.
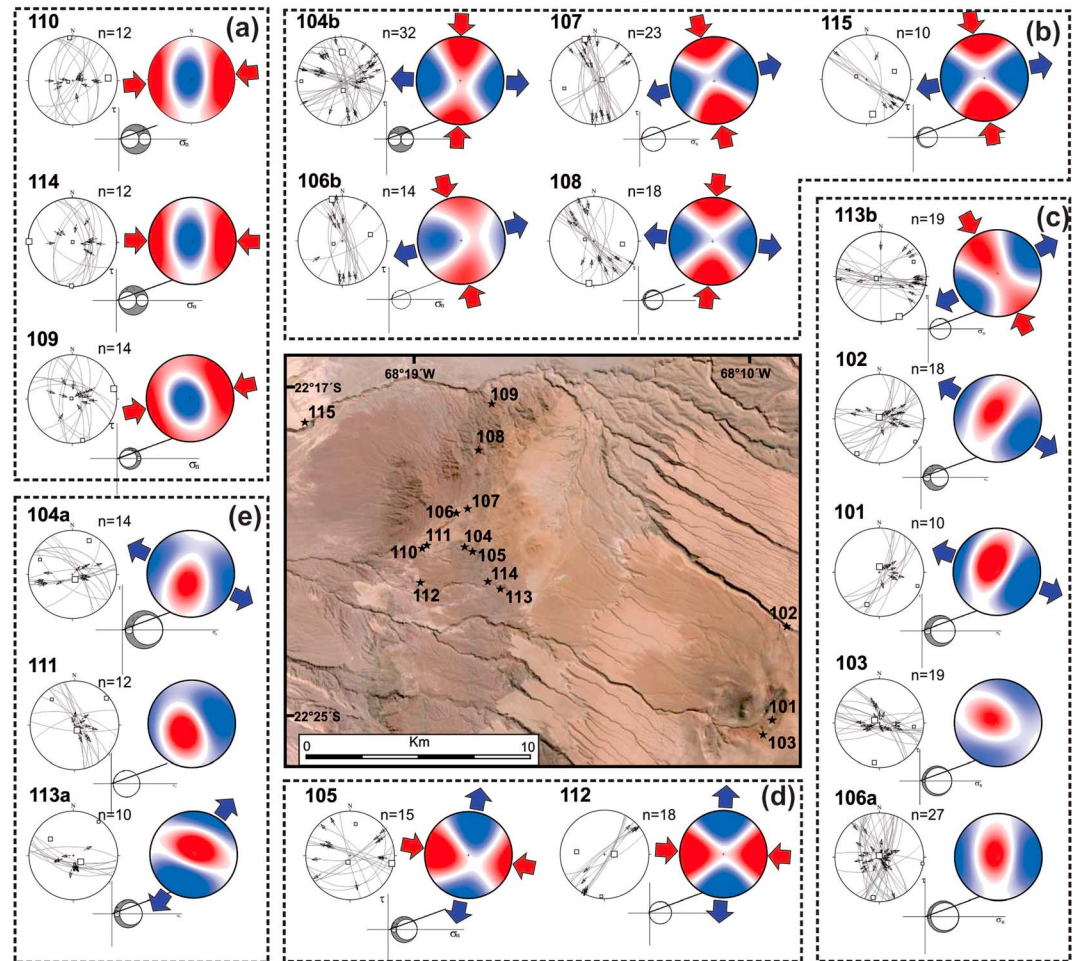
Figure 5. Google Earth image with measurement stations. Location in Figure 2a. Equal-area, lower hemisphere plots of fault slip data and reduced stress tensors for each measurement site. (left) For each site, plots show the measured fault planes (great circles), striae, and slip sense (arrows indicate the hanging wall movement). (right) Plots are the computed principal stress axes obtained using T-TECTO 3.0 software from *Zalohar and Vrabec* [2007]. Mohr diagram illustrates the normal σ_n and shear stress τ on the faults (black point representing the poles to fault planes in the shaded region) and relative values of principal stress magnitudes (σ_1, σ_2, and σ_3). The straight line with equation $\mathcal{T} = \sigma_n \times \tan\phi1$ representing the Amonton's law. The values for stress tensors are given in Table 1.

Olacapato-El Toro, are observed at the study area, affecting the middle Miocene to Pleistocene volcanic rocks. The Capur and Cosor lineaments correspond to NNE to NE striking dextral fault systems, while several WNW striking sinistral strike-slip faults form part of the subcontinental Olacapato-El Toro lineament.

Throughout the region, we identify four deformational events: two strike-slip faulting events and two extensional ones (Figure 7). We were able to assign a timing for these deformational events by studying the Laco iron deposit region (Figures 7a–7c) and the partially eroded Tuyajto volcano (Figures 7d and 7e). In the Laco region, the first and second deformational events affect upper Miocene rocks of 10.5 Ma and 7.7 Ma, respectively, while the third event acts on volcanic rocks dated between 5.9 and 4.4 Ma [*Gardeweg and Ramírez*, 1985], and the fourth event affects volcanic rocks younger than 2.2 Ma. The Plio-Pleistocene Tuyajto volcano is affected by a NW sinistral strike-slip fault (Figures 6 and 7d). Minor faults close to the top of the volcano show a WNW trending extensional direction (Figure 7e).

For the Tuyajto area we obtained 13 reduced stress tensors (Figure 6). The upper Miocene stress field (10.5 to 7.7 Ma) corresponds to a strike-slip to strike-slip/extension event with NNW trending horizontal σ_1 and ESE trending horizontal σ_3 (Figure 6a). One stress tensor with radial extension suggests an age <6.17 Ma (Figure 6b). Stress tensors constrained between 5.9 and 4.4 Ma were obtained in different sites throughout
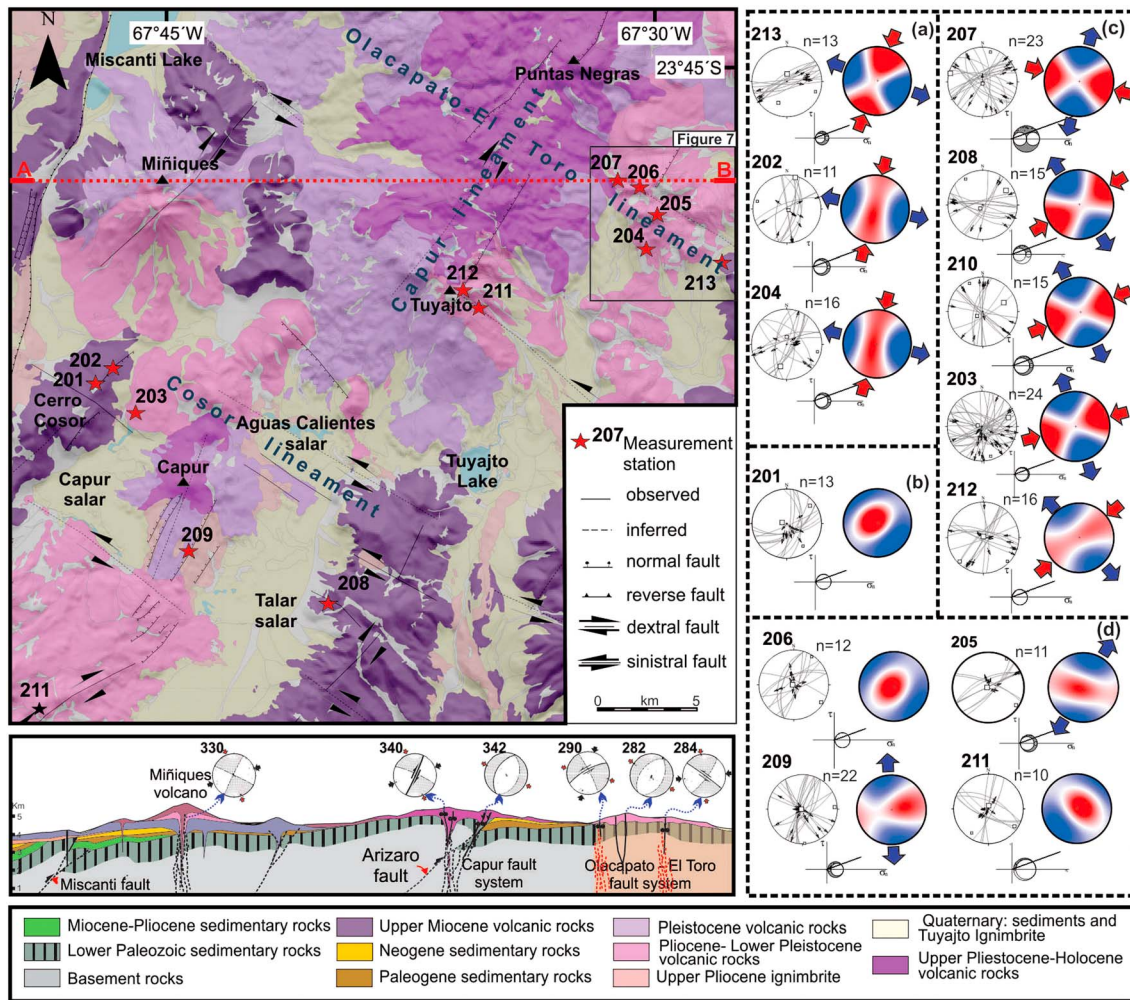
Figure 6. Geological map and cross section of the Tuyajto area (modified from *Gardeweg* [2012]) and equal-area plots of fault slip data and reduced stress tensors results for each measurement site. The data symbols and conventions are same as in Figure 5. Stereonet plots on cross section represent the kinematic of each main fault (see Table S2). (a) Strike-slip to strike-slip/extensional event (10.5–7.7 Ma), (b) radial extension <6.17 Ma, (c) strike-slip and strike-slip/extensional event (5.9–4.4 Ma), and (d) extensional event of Pleistocene to Holocene age.

the area, indicating a strike-slip to strike-slip/extension event, with E-W to WSW trending horizontal σ_1 and N-S to NNW trending horizontal σ_3 (Figure 6c). Stress tensors obtained from mesoscale faults affecting the Pleistocene to Holocene volcanic rocks (<2.2 Ma) correspond to an extensional event with NNW oriented horizontal σ_3 and vertical σ_1 (Figure 6d).

4.3. Juncalito (26°30'S)

At 26–27°S, the Chilean Precordillera involves the east vergent Pedernales fold-and-thrust belt (Figure 8a), which was active since the Upper Cretaceous-Eocene shortening event, and its associated Pedernales fore-land basin [*Cornejo et al.*, 1993]. Eastward of this basin, the Western Cordillera is uplifted by east vergent reverse faults (Figures 8b and 8c). One of these faults is the WNW dipping Aliste thrust which puts Permo-Triassic rocks on top of Oligocene-lower Miocene volcanic rocks, with a E-W to WSW direction of contraction (see supporting information), and is unconformably covered by lower/middle Miocene sedimentary and vol-caniclastic deposits (10–17.5 Ma [*Mpodozis et al.*, 1995]). These deposits are affected by reverse to oblique reverse/strike-slip faults, whose kinematics indicates a NNW direction of shortening.

In this area, we obtained 12 reduced stress tensors (Figure 9) which may be grouped into five types of stress regimes: (1) an early to middle Miocene pure compression (>13 Ma) with west trending horizontal σ_1 and
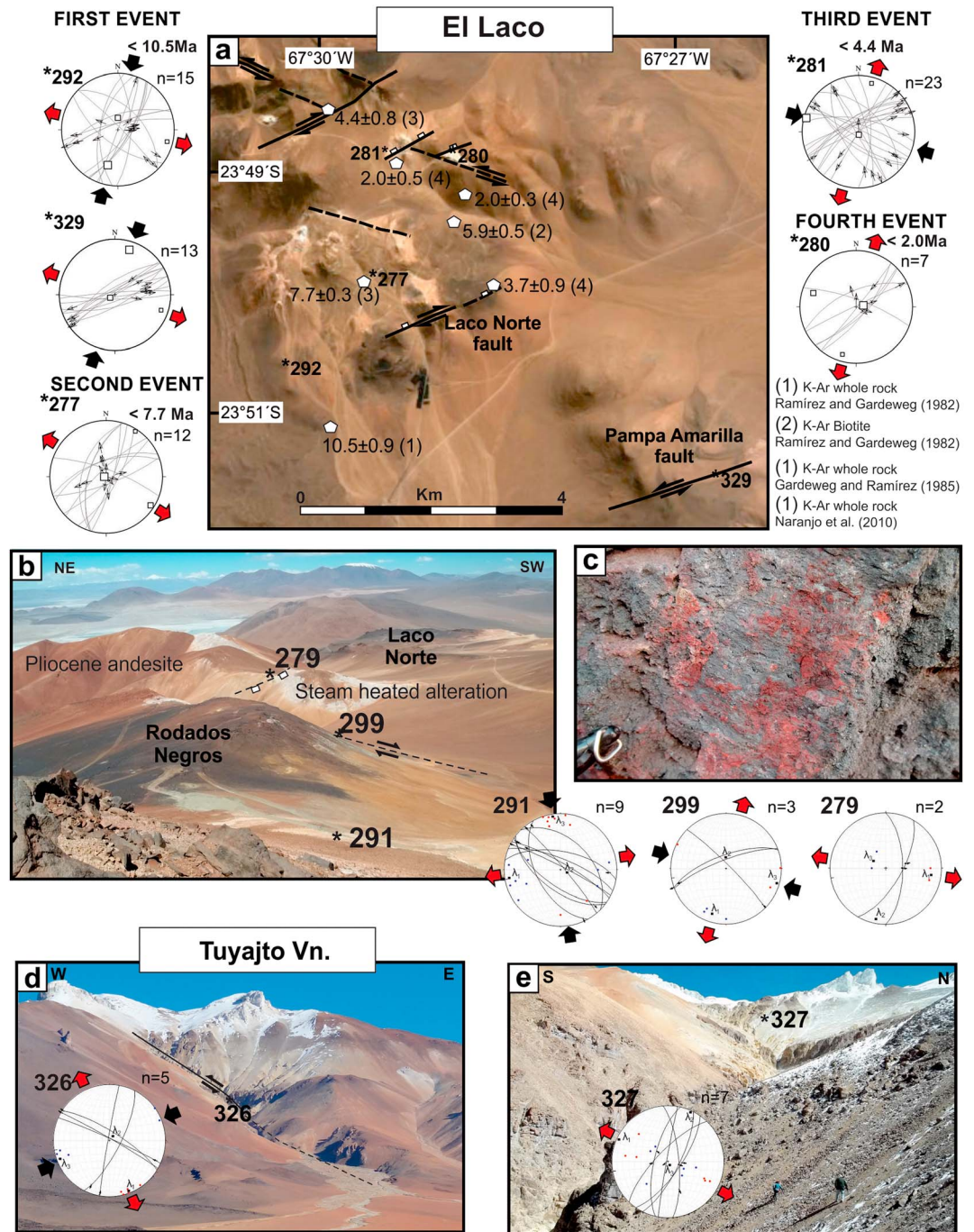
Figure 7. (a) Google Earth image of the El Laco iron deposit and location of measurement stations. The black and red arrows represent the contractional and stretching axes, respectively. (b) Panoramic view of the El Laco deposit. (c) Detailed of striated fault plane with syntectonic hematite fiber growth, indicating a sinistral movement along a NW striking fault. (d) Partially eroded Tuyajto volcano. At station 326 we measured a conjugate system of sinistral NW striking and dextral NNE striking faults. (e). Measurement station at point 327 with mesoscale normal faults affecting the Pleistocene volcanic rocks.

vertical σ_3 (Figure 9a), (2) a late Miocene to early Pliocene compression/strike-slip to strike-slip/extensional event (Figure 9b), (3) a late Pliocene pure extension to extension/strike slip (Figure 9c) with E-W trending σ_3, (4) a late Pliocene pure strike-slip to strike-slip/extensional event (Figure 9d) with N-S extension and E-W compression, and (5) a late Pliocene to Quaternary pure extension (Figure 9e) with σ_3 oriented NNW to NNE.
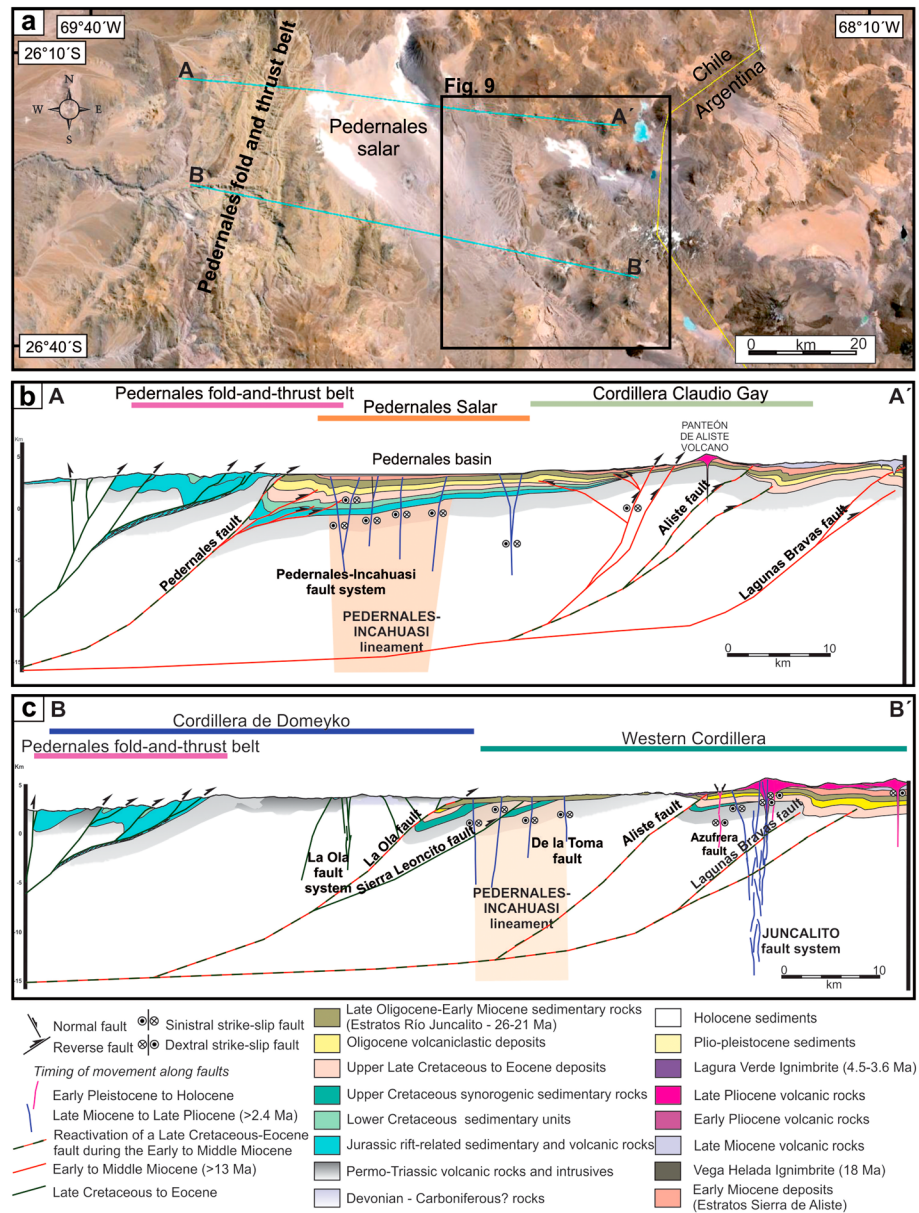
Figure 8. (a) Google Earth image of the Juncalito area and surrounded regions. (b and c) Balanced cross sections crossing the Salar de Pedernales. The study area is located in the Cordillera Claudio Gay.

5. Middle Miocene to Present-Day Stress Patterns in the Western Cordillera (22–26.5°S)

Combining the results from the three study areas, we find consistent stress states, their relative timing, and the transition from one state to the other, allowing us to propose a model of stress field evolution for the Western Cordillera (Figure 10). Out of the 43 reduced stress tensors, 7 indicate pure compression, with a stress ratio close to 0.5, except for 1 tensor, in accordance with the large-scale reverse faults and folds, induced by the Andean tectonic phase. An early to middle Miocene age (20–13 Ma) is assigned for this state of stress in the northern (22°S) and southern (26.5°S) areas. In the central area (24°S) no tensor displays a compressive stress state, due to the age of the outcropping rocks younger than late Miocene. Along the three areas, contraction was not identified in rocks younger than middle Miocene (<13 Ma). Four of the compression tensors have E-W oriented σ_1 (Figure 10a), two indicate a radial compression ($\sigma_1 \sim \sigma_2$; Figure 10b), and one
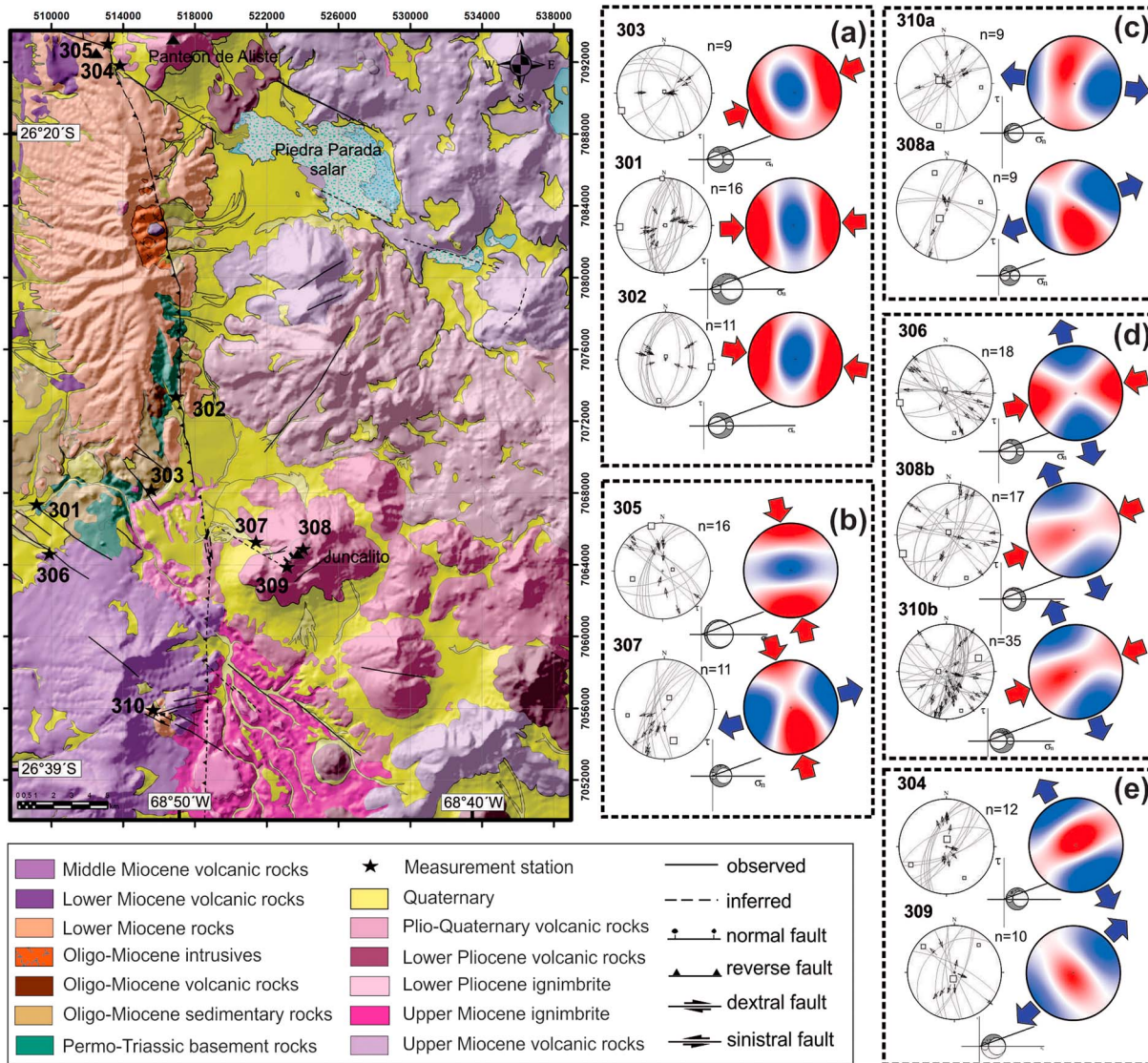
Figure 9. Geological map of the Juncalito area (modified from *Clavero et al.* [1998, 2012]) and equal-area plots of fault slip data and reduced stress tensor results for each measurement site. The data symbols and conventions are the same as in Figure 5.

shows N-S oriented σ_1 (Figure 10c). We interpret this as a reduction in the relative value of SH_{max} (σ_1) with respect to σ_v (σ_3) and SH_{min} (σ_2), associated to a σ_1/σ_2 permutation.

During the late Miocene, compression stopped along the volcanic arc, leading to compression/strike-slip to strike-slip regimes. At the beginning of this phase, the transpressional regime exists, with a NNW to NNE oriented σ_1, represented by 10 of the stress tensors (Figures 10d–10f). The coexistence of compression/strike-slip and strike-slip/compression regimes suggests that these regimes are related to a σ_2/σ_3 stress permutation. Timing for this stress state varies, taking place between ~10 and 7.7 Ma, at the southern Altiplano and northern Puna latitudes (22–24°S) and between 5.5 and 3 Ma at the southern Puna latitudes (26.5°S).

A phase of extension follows the strike-slip event (four stress tensors; Figures 10g and 10h). We associate this phase with a σ_1/σ_2 permutation that leads to an extensional event that finally turns into a radial extension ($\sigma_3 \sim \sigma_2$). A strike-slip event with N-S oriented, subhorizontal σ_3 (10 stress tensors; Figures 10k–10m) is associated with WNW to NW sinistral faults and NNE to ENE dextral faults. This event started in the late Miocene (<6.5 Ma) at 22°S, latest Miocene (<5.9 Ma) at 24°S, and late Pliocene (<2.4 Ma) at 26.5°S, as it is
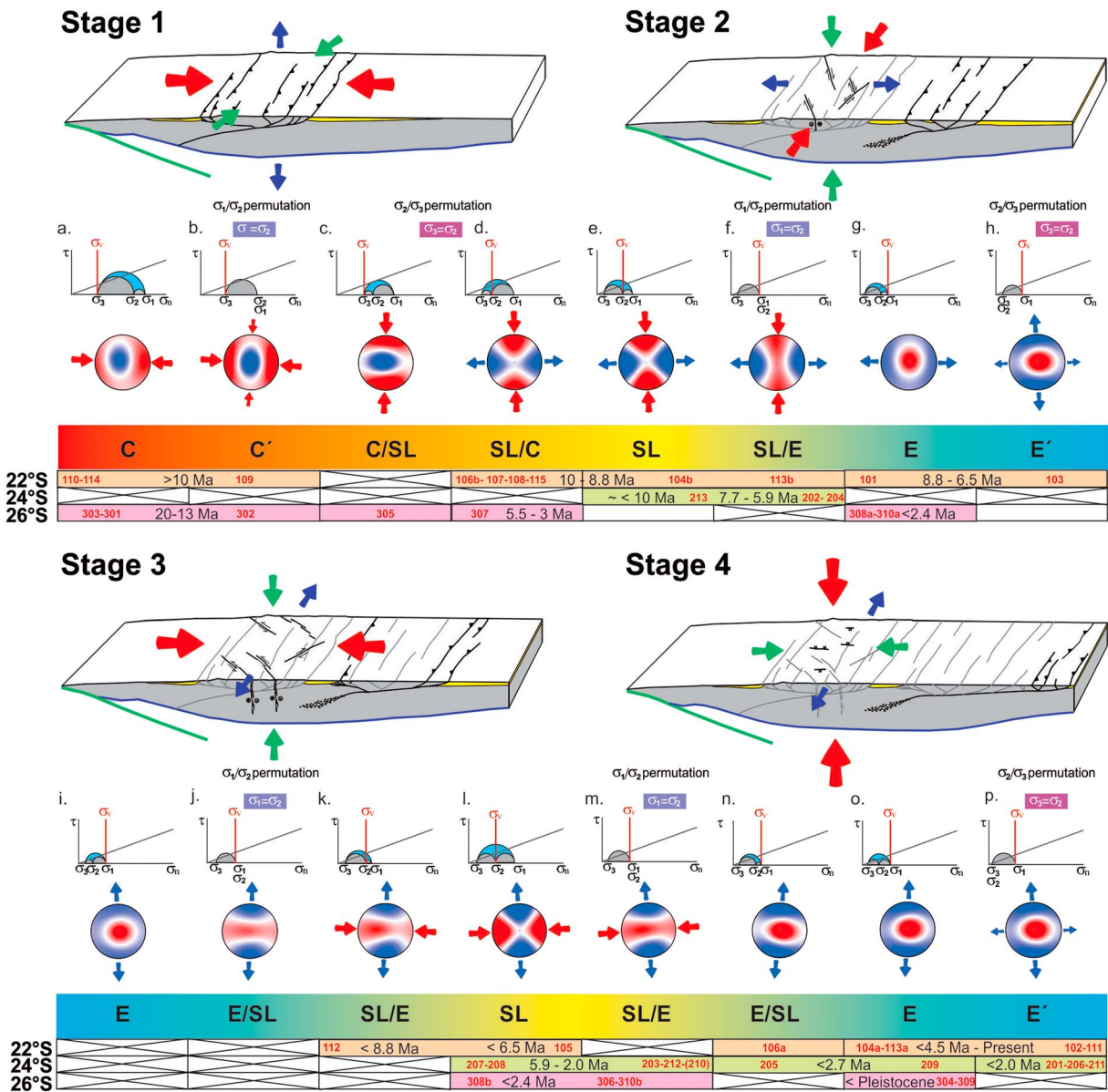
Figure 10. Proposed model of stress field evolution for the Western Cordillera, since the last 20 Myr, with theoretical stress state evolution and summary of timing of stress state for each study area. Each calculated reduced stress tensor with an assigned age is indicated for each study area (22, 24, and 26.5°S) with red numbers. Stress regimes: C pure compression, C' radial compression, C/SL compression/strike slip, SL/C strike slip/compression, SL pure strike slip, SL/E strike slip/extension, E pure extension, and E' radial extension.

indicated by the youngest strata affected by N-S extension and E-W compression. The late Pliocene to Quaternary is characterized by extension along the active volcanic arc (Figures 10n–10p), documented by small (length <5 km), steeply dipping normal faults with highly variable strike. The large majority of the data points to a NNW to NNE oriented σ_3, indicating an orogen-parallel extensional regime, similar to the documented N-S extension in southern and central Perú [*Sébrier et al.*, 1985, 1988b] and northern Perú [*Mercier et al.*, 1992], but other additional tensors indicate E-W oriented σ_3. We speculate that at shallow depths, values of σ_3 and σ_2 get close, and a σ_3/σ_2 permutation is likely. Although, other possibility is that normal north striking faulting could be related to landslide effects, as discussed for the Peruvian Andes where some normal faults are located on the edge of the High Andes [*Sébrier et al.*, 1988b]. This could be the case of the tensor 211 from the Tuyajto area. The radial extension of the tensor 103 from the Paniri area may be related to stress perturbation due to magma intrusion. Other possibility is that data showing radial extension

are biased by mixing fault slip data from more than one episode of extension, such as tensor 310a from Juncalito area obtained from faults affecting middle Miocene rocks. Crosscutting relationship and timing of fault movement for data used to obtain the other radial extension tensors (106a, 111, 201, and 206) indicate that they represent a unique regime with close values of σ_3 and σ_2.

6. Discussion

6.1. Geodynamic Phases and Stress Regimes

We interpret the Miocene to Present stress patterns in the western slope of the Altiplano/Puna plateau in terms of two main geodynamic phases: (1) an orogenic constructional phase, older than late Miocene, and (2) a gravitational collapse phase, active from late Miocene to present. Our results indicate a four-stage stress regime evolution during the transition from one geodynamic phase to the other (Figure 10), in which the dominant E-W compression (stage 1) is followed by a strike-slip event with N-S compression and E-W extension (stage 2), overprinted by a second strike-slip event, but with E-W compression and N-S extension (stage 3), followed by dominant N-S extension (stage 4). Stage 1 corresponds to the orogenic constructional phase, while stages 2, 3, and 4 correspond to the gravitational collapse phase. Our data suggest that the transitions between stages 1 and 2 and between stages 2 and 3 occur in a short-period of time, with the development of E-W striking reverse and oblique/reverse faults and normal and oblique/normal faults, respectively. Between stages 1 and 2, a N-S compression/strike-slip event is documented in the southern area. However, no reverse faulting that could be associated to such stress field was observed in the northern areas. This absence could suggest that differential stresses were too low to fracture the rock under compression but large enough to induce moderate faulting under strike-slip regime.

During the transitions from compressive to strike-slip and from strike-slip to extensional stress fields, the ϕ ratio is close to 0 and 1, respectively. For this reason, σ_1/σ_2 and σ_2/σ_3 stress permutations may be invoked. During these transitions, different faulting regimes may be coeval, such as reverse and strike slip (when σ_2 is close to σ_3) and strike slip and normal (when σ_2 is close to σ_1). We explain these σ_1/σ_2 and σ_2/σ_3 permutations as a decrease in the horizontal stress perpendicular to the orogen, which switches first from σ_1 to σ_2 due to a lateral support of the mountain range and then from σ_2 to σ_3 (Figure 10). This model has been proposed for the Peruvian Andes by *Sébrier et al.* [1988b]. Above the flat-slab segment, these authors pointed out that at a mean elevation higher than 4000 m, the tectonic regime is extensional, while between 3700 and 4000 m compressional strike-slip tectonics occur.

A variety of sources and processes contribute to the stress field within the Andes, being the most important the balance between boundary and body forces. Boundary forces correspond to resistive forces at the subduction zone and ridge push forces from the Atlantic mid-ocean ridge and the portion of the ridge push forces from the Nazca plate transferred at the plate interface. These forces are responsible for the regional stress field [*Assumpção*, 1992]. Topography-induced body forces are generated by the isostatically compensated thickened crust [*Dalmayrac and Molnar*, 1981; *Froidevaux and Isacks*, 1984; *Zoback and Magge*, 1991; *Coblentz and Richardson*, 1996]. Another process that controls the stress field and its evolution is the concentration of horizontal stresses in the upper part of the lithosphere, as a result of heat flow increase and ductile deformation in the lower lithosphere [*Kusznir*, 1991; *Richardson and Coblentz*, 1994] during the thickening of the crust and/or thinning of the lithospheric mantle.

Our model (Figure 10) proposes that permutation of principal stress axes occur during the crustal thickening in the arc region. The average lithospheric vertical stress σ_{zz} increases together with the crustal thickness, and the anomalous low-density mantle beneath [*Fleitout and Froidevaux*, 1982], but in the upper crust, at a certain depth, the vertical stress is maintained constant and equal to the lithostatic load or decrease if we consider erosion of the rock column above. The average lithospheric horizontal stress σ_{xx} generated by the converging plates is maintain constant during the crustal thickening, but locally, the horizontal stress diminishes in the Altiplano/Puna as outward acting buoyancy stresses increase due to gravitation spreading [*Tassara*, 2005]. This is counteracted by an increase in horizontal stress σ_{xx} in the foreland area, resulting in a wider zone of thickened crust and important amount of horizontal shortening in the Subandean ranges. Within linear mountain belts, the reduction in horizontal principal stresses should be considerably more important perpendicular to the orogen than parallel to it, allowing σ_1/σ_2 permutation at a first stage and a σ_2/σ_3 permutation with subsequent gravitational spreading.

The switch from the N-S extension, active during the transition between stages 2 and 3 (Figures 10i and 10j), to the strike-slip regime with N-S extension and W-E compression (Figures 10k–10m), implies either that (i) S_v decreases relative to SH_{max} or (ii) SH_{max} increases related to a nearly constant S_v. A decrease in σ_v may be due to exhumation processes, when the slope of the Western Cordillera acquired its present configuration. However, in the arid to hyperarid, largely unglaciated central Andes denudation processes are minimized [*Strecker et al.*, 2007]. An increase in SH_{max} may be due to an extrinsic factor, such as a change in the regional boundary conditions, for instance, an increase in plate coupling [*Hindle et al.*, 2002], or an intrinsic one, such as the stress concentration in the uppermost crust as the lithosphere gets thermally weaker. Variations in elastic thickness, mainly controlled by lithosphere temperatures and thicknesses, are responsible for variation in horizontal stresses [*Burov and Diament*, 1995; *Tassara et al.*, 2007]. Only the upper elastic part of the crust has significant strength and is involved in transferring tectonic forces. The lower crust and upper mantle, in contrast, may be sufficiently weak to flow under tectonic or gravitational forces [*Hyndman et al.*, 2009]. In regards to this, as the evolution of the orogeny promotes a thinning in the elastic thickness, it produces a concentration of horizontal stresses and an increase in SH_{max} if the boundary forces are maintained nearly constant in the upper crust.

Possible cause for the stress field change in the south central Andes have been previously discussed by Marrett *et al.* [1994], *Cladouhus et al.* [1994], and *Marrett and Strecker* [2000]. *Marrett and Strecker* [2000] argued that the Pliocene reorganization of Pacific plate movement could possibly influence the Nazca-South America dynamics and the kinematic change in the central Andes. Although we do not rule out this factor, our data show that this switch in stress state occurred first in the north and afterward in the south, indicating that an intrinsic process controls it. A possible explanation for this switch is the horizontal stress amplification in the upper lithosphere as a result of an increase in heat flow and a consequent change in the elastic thickness. This reduces the thickness over which the tectonic stress is supported [*Kusznir*, 1991]. Our model suggests that changes in the elastic thicknesses during the construction of the Andean plateau, due to either thickening of the crust or thinning of the lithosphere, generate an increase in the maximum horizontal stress, perpendicular to the orogen.

6.2. Regional Implications

For the southern Altiplano (~22°S), crustal thicknesses between 20 and 15 Ma have been predicted to be <80% of the modern one [*Lamb and Hoke*, 1997; *Hoke and Lamb*, 2007; *Eichelberger et al.*, 2015] and paleoelevation of 50–70% of the modern one [*Garzione et al.*, 2014]. By 10 Ma, crustal thickness is inferred to have achieved its modern value [*Eichelberger et al.*, 2015], with an important surface uplift between 16 and 9 Ma, when the plateau rose to its current elevation [*Garzione et al.*, 2014]. This is in agreement with up to 2 km of surface uplift of the Western Cordillera that took place before 8 Ma [*Farías et al.*, 2005] and the end of long-wavelength deformation affecting the western slope of the Andes between 18 and 27°S [*Hoke et al.*, 2007; *Riquelme et al.*, 2007; *Jordan et al.*, 2010].

Our paleostress analyses of the southern Altiplano (22°S) and northern Puna (24°S) latitudes indicate a change from compression to strike-slip regime between 13 and 10 Ma, suggesting, with an independent parameter, that the crust achieved its maximum thickness and maximum topographic uplift by that time, in clear agreement with paleoelevation studies and models of crustal thickness evolution. The cessation of horizontal contractional deformation at these latitudes is coeval with (1) an eastward shift of thrusting from the Altiplano into the foreland coeval with the underthrusting of the Brazilian Shield [*Suárez et al.*, 1983; *Isacks*, 1988; *Allmendinger and Gubbels*, 1996; *Lamb et al.*, 1997; *McQuarrie*, 2002; *Horton*, 2005; *Elger et al.*, 2005; *Ege et al.*, 2007; *Carrapa et al.*, 2008], (2) the concentration of horizontal shortening in the area to the west of the Western Cordillera that continued at least into the Pleistocene [*Kuhn*, 2002; *Pananont et al.*, 2004; *González et al.*, 2009], and (3) the onset of voluminous ignimbrite-dome complexes related to giant calderas in the region called the Altiplano-Puna Volcanic Complex between 10 and 4 Ma [*de Silva and Gosnold*, 2007].

At the latitudes of the southern Puna (26.5°S), our results show that the stress state changes from compression to strike-slip during the early Pliocene, between 6 and 3 Ma. This is in agreement with topographic uplift associated with lithospheric delamination suggested by *Kay et al.* [1994] to have occurred between 8 and 3 Ma, and with strike-slip and extensional faulting documented in the southern Puna, since at least the late Pliocene [*Cladouhus et al.*, 1994; *Marrett et al.*, 1994; *Daxberger and Riller*, 2015].

Changes in magmatism mimic spatiotemporal changes in the stress tensors obtained in this work, suggesting a close relationship between magmatism, particularly the proportions of crustal and mantle components, and stress field, which governs the magma entrapment times, as was proposed by *Kay et al.* [2013] for the southern Puna latitudes. According to these authors, temporal isotopic change, particularly the increase in ^{87}Sr/^{86}Sr ratios during the 9–5 Ma period, is a reflection of the interaction of magmas with a thickened crust. The change from compression to strike-slip regime, suggested here to have occurred between 6 and 3 Ma, indicates that by ~6 Ma the crust achieved its maximum thickness. This stress regime change also provides a plausible explanation for magma ascent within the crust, as previously proposed by *Riller et al.* [2001]. In the southern Altiplano, *de Silva* [1989] attributed the ignimbrite flare-up to heating by influx of hot asthenospheric mantle below a thickened crust. This influx has been associated either to a steepening of the previously flat slab [*Coira et al.*, 1982; *Kay et al.*, 1999] or/and delamination of eclogitic lower crust with thicknesses ˃50 km and underlying mantle lithosphere [*Kay et al.*, 1994; *de Silva et al.*, 2006], with a consequent topographic uplift [*Garzione et al.*, 2006]. Even though our model does not allow us to discriminate between different processes that generate topographic uplift, we suggest that the most powerful mechanism is crustal thickening, although others forces related to changes in the lithospheric mantle by thinning [*Houseman et al.*, 1981; *England and Houseman*, 1989; *Molnar et al.*, 1993; *Garzione et al.*, 2006] may contribute to it.

The geodynamic phases proposed here may be correlated with the two sets of principal strain axis configuration proposed by *Daxberger and Riller* [2015] for the Neogene evolution of the Puna and Eastern Cordillera between 23 and 28°S. These authors suggest a first set of configurations characterized by WNW horizontal shortening and vertical extension and a second set with variable horizontal extension and vertical shortening. *Lanza et al.* [2013] present similar results for spatial-temporal variation in the stress field along the Olacapato-El Toro lineament, eastward of the Tuyajto area. Interestedly, these authors suggest the existence of an extensional phase, occurring after the compressional one of >9 Ma, followed by a E-W compression, N-S extension strike-slip regime, in agreement with our results.

At a subcontinental scale, paleostress analyses carried out along the Andes of southern and central Perú show that compressional deformation occurs since the last 1 or 2 Ma on both edges of the Andes, whereas the High Andes exhibits extensional deformation [*Sébrier et al.*, 1985, 1988b]. Seismicity here is generally low [*Sébrier et al.*, 1988b], similar to what occurs in the Altiplano-Puna [*Allmendinger et al.*, 1997]. The main difference between the Chilean Western Cordillera and the Peruvian High Andes is the importance and scale of the extensional deformation in this latter. The extensional deformation in the Peruvian Andes is dominated by large-scale normal faults, such as the 200 km long Cordillera Blanca fault [*Sébrier et al.*, 1988b; *McNulty and Farber*, 2002]. As oppose to this, at the Altiplano/Puna plateau, only small-scale faults can be observed. This reinforces the idea that in the Andean plateau, the balance between compressive forces and body forces results in a neutral to extensional stress state [*Allmendinger et al.*, 1997] and that driving plate tectonic forces maintain the Andean plateau uplifted, supported by the cold and rigid fore arc acting as an indenter against the thermally weakened Altiplano [*Tassara*, 2005].

The evolution of the stress field in Perú and Bolivia for the last 6 Ma indicates that late Miocene E-W compression [*Sébrier et al.*, 1988a] was followed by E-W to NE-SW extension during the Pliocene [*Mercier et al.*, 1992]. Our data indicate a similar scenario for the Western Cordillera (stage 2). In Northern Perú and in the eastern slope of the Bolivian Altiplano, *Mercier et al.* [1992] present evidence for an early Pleistocene compressional regime with E-W compression followed by N-S compression. This change in σ_1 direction from E-W to N-S is similar to our proposed transition between stage 1 and 2, although it is younger in northern Perú. These authors propose that this is the result of the flattening of the slab below the northern Peruvian Andes. To the south, above the normal subduction segment, this late compression in the High Andes is not registered.

7. Conclusions

The geodynamic history of the western slope of the Altiplano/Puna plateau between 22 and 26.5°S for the last 20 Myr can be described in terms of two main geodynamic phases: (1) the orogenic constructional phase and (2) the gravitational collapse of the orogen. We present evidence that the stress field changed significantly during this period and relate this to intrinsic mechanisms of the orogen during its construction. Our paleostress analysis indicates that the tectonic regime varied from compression to strike-slip to extension, with the transition from one regime to another due to the permutation of either σ_1/σ_2 or σ_2/σ_3.

Comparing the results of our three study areas, we observe close similarities in the stress field evolution between southern Altiplano and northern Puna western slopes but major differences along the southern Puna sector. Taking into account our results, we propose that the achievement of the maximum crustal thickness at ~13–10 Ma, for the 22–24°S segment, and at ~6 Ma at 26.5°S, explains the transition between the two proposed geodynamic phases. This transition is marked by four stress states. During the first stage, the direction of σ_1 indicates compression near the east-west direction and a stress ratio close to 0.5 during the 20–13 Ma period. This E-W compression leads place to a N-S compression, and then to a strike-slip regimes with N-S oriented σ_2, and vertical σ_1, suggesting a permutation between σ_1/σ_2, first, and a σ_2/σ_3, afterward.

The transition from the orogenic constructional phase to the gravitational collapse one was controlled by intrinsic factors. The most important of these factors are (1) the achievement in a threshold value of crustal thickness that the orogen was able to gain under the specific boundary conditions and (2) the reduction of the elastic thickness as a result of thermal state changes. The results of this study emphasize the role played by intrinsic processes, such a thickening of the crust, thinning of the mantle lithosphere, and thinning of the elastic thickness, associated with the construction of the Andean orogeny, in the evolution of the stress field.

References

Acocella, V., A. Gioncada, R. Omarini, U. Riller, R. Mazzuoli, and L. Vezzoli (2011), Tectonomagmatic characteristics of the back-arc portion of the Calama-Olacapato-El Toro fault zone, central Andes, *Tectonics*, *30*, TC3005, doi:10.1029/2010TC002854.

Allmendinger, R. W. (2001), FaultKinWinFull versión 1.2.2. A program for analyzing fault slip data for Windows™ computers. [Available at http://www.geo.cornell.edu/ geology/ faculty/RWA/programs.html.]

Allmendinger, R. W., and T. Gubbels (1996), Pure and simple shear plateau uplift—Puna, Argentina and Bolivia, *Tectonophysics*, *259*, 1–13, doi:10.1016/0040-1951(96)00024-8.

Allmendinger, R. W., V. A. Ramos, T. E. Jordan, M. Palma, and B. Isacks (1983), Paleogeography and Andaean structural geometry, north-west Argentina, *Tectonics*, *2*, 1–16, doi:10.1029/TC002i001p00001.

Allmendinger, R. W., M. Strecker, J. E. Eremchuk, and P. Francis (1989), Neotectonic deformation of the southern Puna Plateau, northwestern Argentina, *J. South Am. Earth Sci.*, *2*, 111–130.

Allmendinger, R. W., T. E. Jordan, S. M. Kay, and B. L. Isacks (1997), The evolution of the Altiplano-Puna plateau of the central Andes, *Annu. Rev. Earth Planet. Sci.*, *25*, 139–174.

Arriagada, C., P. Roperch, C. Mpodozis, G. Dupont-nivet, P. Cobbold, A. Chauvin, and J. Cortés (2003), Paleogene clockwise tectonic rotations in the forearc of central Andes, Antofagasta region, northern Chile, *J. Geophys. Res.*, *108*(B1), 2031, doi:10.1029/2001JB001598.

Artyushkov, E. V. (1973), Stresses in the lithosphere caused by crustal thickness inhomogeneities, *J. Geophys. Res.*, *78*, 7675–7708, doi:10.1029/JB078i032p07675.

Assumpção, M. (1992), The regional intraplate stress field in South America, *J. Geophys. Res.*, *97*, 11,889–11,903, doi:10.1029/91JB01590.

Assumpção, M., and M. Araujo (1993), Effect of the Altiplano-Puna plateau, South America, on the regional intraplate stresses, *Tectonophysics*, *221*, 457–495.

Barke, R., and S. Lamb (2006), Late Cenozoic uplift of the Eastern Cordillera, Bolivian Andes, *Earth Planet. Sci. Lett.*, *249*, 350–367.

Beck, S., and G. Zandt (2002), The nature of orogenic crust in the central Andes, *J. Geophys. Res.*, *107*(B10), 2230, doi:10.1029/2000JB000124.

Blanco, N., and A. Tomlinson (2009), Carta Chiu Chiu, Región de Antofagasta, Carta Geológica de Chile, *Ser. Geol. Básica*, *117*, 54 p., Serv. Nac. De Geol. y Minería, Santiago.

Bonali, F. L., C. Corazzato, and A. Tibaldi (2012), Elastic stress interaction between faulting and volcanism in the Olacapato-San Antonio de Los Cobres area (Puna plateau, Argentina), *Global Planet. Change*, *90-91*(104), 120.

Burov, E. B., and M. Diament (1995), The effective elastic thickness (T_e) of continental lithosphere: What does it really mean?, *J. Geophys. Res.*, *100*, 3,905–3,927, doi:10.1029/94JB02770.

Carrapa, B., M. R. Strecker, and E. R. Sobel (2008), Cenozoic orogenic growth in the central Andes: Evidence from sedimentary rock provenance and apatite fission track thermochronology in the Fiambalá basin, southernmost Puna Plateau margin (NW Argentina), *Earth Planet. Sci. Lett.*, *247*, 82–100.

Chernicoff, C., J. P. Richards, and E. O. Zappettini (2002), Crustal lineament control on magmatism and mineralization in northwestern Argentina: Geological, geophysical, and remote sensing evidence, *Ore Geol. Rev.*, *21*, 127–155.

Cladouhus, I. T., R. W. Allmendinger, B. Coira, and E. Farrar (1994), Late Cenozoic deformations in the central Andes: Fault kinematics from the northern Puna, northwest Argentina and southwest Bolivia, *J. South Am. Earth Sci.*, *7*, 209–228, doi:10.1016/0895-9811(94)90008-6.

Clavero, J., M. Gardeweg, and C. Mpodozis (1998), Mapa Geológico del área del Salar de Piedra Parada, Región de Atacama, 1:100.000 (Inedito), Servicio Nacional de Geología y Minería, Santiago, Chile.

Clavero, J., R. Arcos, and E. Polanco (2012), Mapa geológico concesión de Explotación ENERGIA Geotérmica Juncalito. 1:100000. Informe inédito Energía Andina

Coblentz, D. D., and R. M. Richardson (1996), Analysis of the South American intraplate stress field, *J. Geophys. Res.*, *101*, 8643–8657, doi:10.1029/96JB00090.

Coira, B., J. Davidson, C. Mpodozis, and V. A. Ramos (1982), Tectonic and magmatic evolution of the Andes of northern Argentina and Chile, *Earth Sci. Rev.*, *18*, 303–322.

Cornejo, P., C. Mpodozis, C. Ramirez, and A. Tomlinson (1993), Estudio geológico de la región de Potrerillos y El Salvador (26-27°S). SERNAGEOMIN-CODELCO, Informe Registrado IR-93 01, 1:50.000, Santiago, Chile, 258 p.

Dalmayrac, B., and P. Molnar (1981), Parallel thrust and normal faulting in Peru and constraints on the state of stress, *Earth Planet. Sci. Lett.*, *55*, 473–481.

Daxberger, H., and U. Riller (2015), Kinematics of Neogene to Recent upper-crustal deformation in the southern central Andes (23°-28°S) inferred from fault-slip analysis: Evidence for gravitational spreading of the Puna Plateau, *Tectonophysics*, *642*, 16–28, doi:10.1016/j.tecto.2014.12.003.

De Silva, S. L. (1989), Altiplano-Puna volcanic complex of the central Andes, *Geology*, *17*, 1102–1106.

De Silva, S. L., and W. Gosnold (2007), Cordilleran Batholith development: Insights from an ignimbrite flare-up, *J. Volcan. Geoth. Res.*, *167*, 320–335.

De Silva, S., G. Zandt, R. Trumbull, J. G. Viramonte, G. Salas, and N. Jiménez (2006), Large ignimbrite eruptions and volcano-tectonic depressions in the central Andes: A thermomechanical perspective, in *Mechanism of Activity and Unrest at Large Claderas*, edited by C. Troise, G. De Natale, and C. R. Kilburn , *Geol. Soc. Spec. Publ.*, *269*, 47–63.

Delvaux, D., R. Moeys, G. Stapel, C. Petit, K. Levi, A. Miroshnichenko, V. Ruzhich, and V. San'kov (1997), Paleostress reconstructions and geodynamics of the Baikal region, central Asia, Part 2. Cenozoic rifting, *Tectonophysics*, *282*, 1–38.

DeMets, C., R. G. Gordon, D. F. Argus, and S. Stein (1994), Effect of recent revisions on to the geomagnetic reversal time scale on estimates of current plate motions, *Geophys. Res. Lett.*, *21*, 2191–2194, doi:10.1029/94GL02118.

Ege, H. E., R. Sobel, E. Scheuber, and V. Jacobshagen (2007), Exhumation history of the southern Altiplano plateau (southern Bolivia) constrained by apatite fission track thermochronolgoy, *Tectonics*, *26*, TC1004, doi:10.1029/2005TC001869.

Eichelberger, N., N. McQuarrie, J. Ryan, B. Karimi, S. Beck, and G. Zandt (2015), Evolution of crustal thickening in the central Andes, Bolivia, *Earth Planet. Sci. Lett.*, *426*, 191–203.

Elger, K., O. Oncken, and J. Glodny (2005), Plateau-style accumulation of deformation: Southern Altiplano, *Tectonics*, *24*, TC4020, doi:10.1029/2004TC001675.

England, P., and G. Houseman (1989), Extension during continental convergence, with applicagtion to the Tibetan Plateau, *J. Geophys. Res.*, *94*, 17,561–17,579, doi:10.1029/JB094iB12p17561.

Farías, M., R. Charrier, D. Comte, J. Martinod, and G. Hérail (2005), Late Cenozoic deformation and uplift of the western flank of the Altiplano: Evidence from the depositional, tectonic, and geomorphologic evolution and shallow seismic activity (northern Chile at 19°30'S), *Tectonics*, *24*, TC4001, doi:10.1029/2004TC001667.

Fleitout, L., and C. Froidevaux (1982), Tectonics and topography for a lithosphere containing density heterogeneities, *Tectonics*, *1*, 21–56, doi:10.1029/TC001i001p00021.

Froidevaux, C., and B. I. Isacks (1984), The mechanical state of the lithosphere in the Altiplano-Puna segment of the Andes, *Earth Planet. Sci. Lett.*, *71*, 305–314.

Gardeweg, M. (2012), Geologia de las concesiones Tuyajto 1, 2 y 3, Región de Antofagasta Chile. Unpublished map, 1:75.000, Informe interno de Energía Andina Chile.

Gardeweg, M., and C. F. Ramírez (1985), Hoja Río Zapaleri, II Región de Antofagasta, Santiago, Chile, Sernageomin, Geol map 66, 89 p.

Garzione, C. N., P. Molnar, J. C. Libark, and B. J. MacFadden (2006), Rapid late Miocene rise of the Bolivian Altiplano: Evidence for removal of mantle lithosphere, *Earth Planet. Sci. Lett.*, *241*, 543–556, doi:10.1016/j.epsl.2005.11.026.

Garzione, C. N., G. D. Hoke, J. C. Libarkin, S. Withers, B. MacFadden, J. Eiler, P. Ghosh, and A. Mulch (2014), Rise of the Andes, *Science*, *320*, 1304–1307.

Giambiagi, L., et al. (2015), Evolution of shallow and deep structures along the Maipo-Tunuyán transect (33°40'S): From the Pacific coast to the Andean foreland, in *Geodynamic Processes in the Andes of Central Chile and Argentina*, edited by S. Sepúlveda et al., *Geol. Soc. London, Spec Publ.*, 399, 63–82. doi:10.1144/SP399.14.

González, G., J. Cembrano, F. Aron, E. Veloso, and B. Shyu (2009), Coeval compressional deformation and volcanism in the central Andes, case studies from northern Chile (23°-24°S), *Tectonics*, *28*, TC6003, doi:10.1029/2009TC002538.

Gordon, R. G., and D. M. Jurdy (1986), Cenozoic global plate motion, *J. Geophys. Res.*, *91*, 12,389–12,406, doi:10.1029/JB091iB12p12389.

Gudmundsson, A. (2006), How local stresses control magma-chamber ruptures, dyke injections, and eruptions in composite volcanoes, *Earth Sci. Rev.*, *79*, 1–31.

Heidbach, O., G. Iaffaldano, and H. P. Bunge (2008a), Topography growth drives stress rotations in the central Andes: Observations and models, *Geophys. Res. Lett.*, *35*, L08301, doi:10.1029/2007GL032782.

Heidbach, O., M. Tingay, A. Barth, J. Reinecker, D. Kurfeß, and B. Müller (2008b), The World Stress Map database release 2008, doi:10.1594/GFZ.WSM.Rel2008.

Hindle, D., J. Kley, E. Klosko, S. Stein, T. Dixon, and E. Norabuena (2002), Consistency of geologic and geodetic displacements during Andean orogenesis, *Geophys. Res. Lett.*, *29*(8), 1188, doi:10.1029/2001GL013757.

Hoke, L., and S. H. Lamb (2007), Cenozoic behind-arc volcanism in the Bolivian Andes, South America: Implications for mantle melt generation and lithospheric structure, *J. Geol. Soc., London*, *164*, 795–814.

Hoke, G. D., B. L. Isacks, T. E. Jordan, N. Blanco, A. J. Tomlinson, and J. Ramezani (2007), Geomorphic evidence of post-10 Ma uplift of the western flank of the central Andes at 18°30'22"S, *Tectonics*, *26*, TC5021, doi:10.1029/2006TC002082.

Hoke, G. D., L. Giambiagi, C. Garzione, B. Mahoney, and M. Strecker (2014), Neogene paleoelevation of intermontane basins in a narrow, compressional mountain range, southern central Andes of Argentina, *Earth Planet. Sci. Lett.*, *406*, 153–164.

Horton, B. K. (2005), Revised deformation history of the central Andes: Inferences from Cenozoic foredeep and intermontane basins of the Eastern Cordillera, Bolivia, *Tectonics*, *24*, TC3011, doi:10.1029/2003TC001619.

Houseman, G. A., D. P. McKenzie, and P. Molnar (1981), Convective instability of a thickened boundary layer and its relevance for the thermal evolution of continental convergent belts, *J. Geophys. Res.*, *86*, 6115–6132, doi:10.1029/JB086iB07p06115.

Hyndman, R. D., C. A. Currie, S. Mazzotti, and A. Frederiksen (2009), Temperature control of continental lithosphere elastic thickness, T_e vs V_s, *Earth Planet Sc. Lett.*, *277*, 539–548.

Iaffaldano, G., H.-P. Bunge, and T. Dixon (2006), Feedback between mountain belt growth and plate convergence, *Geology*, *34*, 893–896, doi:10.1130/G22661.1.

Isacks, B. L. (1988), Uplift of the central Andean plateau and bending of the Bolivian orocline, *J. Geophys. Res.*, *93*, 3211–3231, doi:10.1029/JB093iB04p03211.

Jordan, T. E., P. L. Nester, N. Blanco, G. D. Hoke, F. Dávila, and A. J. Tomlinson (2010), Uplift of the Altiplano-Puna plateau: A view from the west, *Tectonics 29*, TC5007, doi:10.1029/2010TC002661.

Kaven, J. O., F. Maerten, and D. D. Pollard (2011), Mechanical analysis of fault slip data: Implications for paleostress analysis, *J. Struct. Geol.*, *33*, 78–91.

Kay, S. M., B. Coira, and J. Viramonte (1994), Young mafic back arc volcanic rocks as indicators of continental lithospheric delamination beneath the Argentine Puna Plateau, central Andes, *J. Geophys. Res.*, *99*, 24,323–24,339, doi:10.1029/94JB00896.

Kay, S. M., C. Mpodozis, and B. Coira (1999), Magmatism, tectonism, and mineral deposits of the central Andes (22°-33°S latitudes), in *Geology and Ore Deposits of the Central Andes*, *Spec. Publ. Soc. Econ. Geol.*, vol. 7, edited by B. Skinner, pp. 27–59, Society of Economic Geologists, Littleton.

Kay, S. M., C. Mpodozis, and M. Gardeweg (2013), Magma sources and tectonic setting of central Andean andesites (25.5-28°S) related to crustal thickening, forearc subduction erosion and delamination, in *Orogenic Andesites and Crustal Growth*, edited by A. Gómez-Tuela, S. M. Straub, and G. F. Zellmer, *Geol. Soc. London, Spec. Publ.*, 385, 303–334, doi:10.1144/SP385.11.

Kuhn, D. (2002), Fold and thrust belt structures and strike-slip faulting at the SE margin of the Salar de Atacama basin, Chilean Andes, *Tectonics*, *21*(4), 1026, doi:10.1029/2001TC901042.

Kusznir, N. (1991), The distribution of stress with depth in the lithosphere: Thermo-rheological and geodynamic constraints, in *Tectonic Stress in the Lithosphere*, edited by R. B. Whitmarsh et al., pp. 95–110, R. Soc., London.

Lacombe, O. (2012), Do fault slip data inversions actually yield "paleostresses" that can be compared with contemporary stresses? A critical discussion, *C. R. Geosci.*, *344*, 159–173.

Lamb, S. H., and L. Hoke (1997), Origin of the high plateau in the central Andes, Bolivia, South America, *Tectonics*, *16*, 623–647, doi:10.1029/97TC00495.

Lamb, S., L. Hoke, L. Kennan, and J. Dewey (1997), Cenozoic evolution of the central Andes in Bolivia and northern Chile, in *Orogeny Through Time*, edited by J.–P. Burg and M. Ford, *Geol. Soc. London, Spec. Publ.*, 121, 237–264.

Lanza, F., A. Tibaldi, F. L. Bonali, and C. Corazzato (2013), Space-time variations of stresses in the Miocene-Quaternary along the Calama-Olacapato-El Toro fault zone, central Andes, *Tectonophysics*, *593*, 33,56.

Lahsen, A., and F. Munizaga (1979), Nuevos antecedentes cronológicos del volcanismo cenozoico superior de los Andes del norte de Chile, entre los 19°00′ y los 22°30′ lat. S. In Congreso Geológico Chileno, No. 2, Actas, Vol. 1, p. F61–F82.

Marinovic, N., and A. Lahsen (1984), Hoja Calama, Carta geológica de Chile, Escala 1:250.000, Servicio Nacional de Geología y Mineraía, Carta No. 58, Santiago, Chile.

Marrett, R., and M. R. Strecker (2000), Response of intracontinental deformation in the central Andes to the late Cenozoic reorganization of South American Plate motions, *Tectonics*, *19*, 452–467, doi:10.1029/1999TC001102.

Marrett, R. A., R. W. Allmendinger, R. N. Alonso, and R. E. Drake (1994), Late Cenozoic tectonic evolution of the Puna Plateau and adjacent foreland, northwestern Argentine Andes, *J. South Amer. Earth Sci.*, *7*, 179–207.

Matteini, M., R. Mazzuoli, R. Omarini, R. A. Cas, and R. Maas (2002), Geodynamical evolution of the central Andes at 24°S as inferred by magma composition along the Calama-Olacapato-El Toro transversal volcanic belt, *J. Volcanol. Geotherm. Res.*, *118*, 205–228, doi:10.1016/S0377-0273(02)00257-3.

McGlashan, N., L. D. Brown, and S. M. Kay (2008), Crustal thicknesses in the central Andes from teleseismically recorded depth phase precursors, *Geoph. J. Int.*, *175*, 1013–1022.

McNulty, B., and D. Farber (2002), Active detachment faulting above the Peruvian flat slab, *Geology*, *30*, 567–570.

McQuarrie, N. (2002), Building a high plateau: The kinematic history of the central Andean fold-thrust belt, Bolivia, *Geol. Soc. Am. Bull.*, *114*, 950–963.

Mercier, J.-L. (1981), Extensional-compressional tectonics associated with the Aegean arc; Comparison with the Andean cordillera of south Peru-north Bolivia, *Philos. Trans. R. Soc. London*, A300, 337–355.

Mercier, J.-L., M. Sébrier, A. Lavenu, J. Cabrera, O. Bellier, J.-F. Dumont, and J. Machare (1992), Changes in the tectonic regime above a subduction zone of Andean type: The Andes of Perú and Bolivia during the Pliocene-Pleistocene, *J. Geophys. Res.*, *97*, 11,945–11,982, doi:10.1029/90JB02473.

Molnar, P., and H. Lyon-Caen (1988), Some simple physical aspects of the support, structure, and evolution of mountain belts, *Geol. Soc. Am. Spec. Pap.*, *218*, 179–207.

Molnar, P., and P. Tapponnier (1978), Active tectonics of Tibet, *J. Geophys. Res.*, *83*, 5361–5375, doi:10.1029/JB083iB11p05361.

Molnar, P., P. England, and J. Martinod (1993), Mantle dynamics, the uplift of the Tibetan Plateau, and the Indian monsoon, *Rev. Geophys.*, *31*, 107–114, doi:10.1029/93RG02030.

Mpodozis, C., P. Cornejo, S. M. Kay, and A. Tittler (1995), La Franja de Maricunga: Síntesis de la evolución del frente volcánico Oligoceno-Mioceno en la zona sur de los Andes centrales, *Rev. Geol. Chile*, *22*, 273–313.

Mpodozis, C., C. Arriagada, M. Basso, P. Roperch, P. Cobbold, and M. Reich (2005), Late Mesozoic to Paleogene stratigraphy of the Salar de Atacama Basin, Antofagasta, northern Chile: Implications for the tectonic evolution of the central Andes, *Tectonophysics*, *399*, 125–154, doi:10.1016/j.tecto.2004.12.019.

Naranjo, J. A., F. Henríquez, and J. O. Nyström (2010), Subvolcanic contact metasomatism at El Laco Volcanic Complex, central Andes, *Andean Geol.*, *37*, 110–120.

Pananont, P., C. Mpodozis, N. Blanco, T. E. Jordan, and L. D. Brown (2004), Cenozoic evolution of the northwestern Salar de Atacama basin, northern Chile, *Tectonics*, *23*, TC6007, doi:10.1029/2003TC001595.

Petrinovic, I. A., U. Riller, G. Alvarado, J. A. Brod, and M. Arnosio (2006), Bimodal volcanism in a tectonic transfer zone: Evidence for tectonically controlled magmatism in the southern central Andes, NW Argentina, *J. Volcanol. Geotherm. Res.*, *152*, 240–252.

Polanco, E., J. Clavero, and A. Giavelli (2015), Geología de la cadena volcánica Paniri-Toconce, Zona Volcánica central, Altiplano de la Región de Antofagasta, Chile. XIII Congreso Geologico Chileno, Antofagasta, 463-464.

Ramírez, CF, and M. Gardeweg (1982), Hoja Toconao, Región de Antofagasta. Serv Nac Geol Min Carta Geol de Chile. 54, 122.

Richardson, R. M., and D. J. Coblentz (1994), Stress modeling in the Andes: Constraints on the South American intraplate stress magnitude, *J. Geophys. Res.*, *99*, 22,015–22,025, doi:10.1029/94JB01751.

Riquelme, R., G. Hérail, J. Martinod, R. Charrier, and J. Darrozes (2007), Late Cenozoic geomorphologic signal of Andean forearc deformation and tilting associated with the uplift and climate changes at the Southern Atacama Desert (26°-28°S), *Geomorphology*, *86*, 283–306, doi:10.1016/j.geomorph.2006.09.004.

Riller, U., I. Petrinovic, J. Ramelow, M. Strecker, and O. Onken (2001), Late Cenozoic tectonism, collapse caldera and plateau formation in the central Andes, *Earth Planet. Sci. Lett.*, *188*, 299–311, doi:10.1016/S0012-812X(01)00333-8.

Salfity, J. A. (1985), Lineamientos transversales al rumbo andino en el noroeste argentine, in *Actas IV Congreso Geológico Chileno*, vol. 2, pp. 119–137, Asoc. Geol. Chilena, Antofagasta, Chile.

Salisbury, M. J., B. R. Jicha, S. L. de Silva, B. S. Singer, N. C. Jiménez, and M. H. Ort (2011), [40]Ar/[39]Ar chronostratigraphy of Altiplano-Puna volcanic complex ignimbrites reveals the development of a major magmatic province, *Geol. Soc. Am. Bull.*, *123*, 821–840, doi:10.1130/B30280.1.

Sébrier, M., J. L. Mercier, F. Mégard, G. Laubacher, and E. Carey-Gailhardis (1985), Quaternary normal and reverse faulting and the state of stress in the central Andes of south Peru, *Tectonics*, *4*, 739–780, doi:10.1029/TC004i007p00739.

Sébrier, M., A. Lavenu, M. Fornari, and J. P. Soulas (1988a), Tectonics and uplift in central Andes (Perú, Bolivia and northern Chile) from Eocene to Present, *Geodynamique*, *3*, 85–106.

Sébrier, M., J. L. Mercier, J. Macharé, D. Bonnot, J. Cabrera, and J. L. Blanc (1988b), The state of stress in an overriding plate situated above a flat slab: The Andes of central Perú, *Tectonics*, *7*, 895–928, doi:10.1029/TC007i004p00895.

Sella, G., T. Dixon, and A. Mao (2002), REVEL: A model for Recent plate velocities from space geodesy, *J. Geophys. Res.*, *107*(B4), 2081, doi:10.1029/2000JB000033.

Somoza, R., and A. Tomlinson (2002), Paleomagnetism in the Precordillera of northern Chile (22°30′S): Implications for the history of tectonic rotations in the central Andes, *Earth Planet. Sci. Lett.*, *194*, 369–381.

Strecker, M., R. Alonso, B. Bookhagen, B. Carrapa, G. E. Hilley, E. R. Sobel, and M. H. Trauth (2007), Tectonics and climate of the southern central Andes, *Annu. Rev. Earth Planet. Sci.*, *35*, 747–787, doi:10.1146/annurev.earth.35.031306.140158.

Suárez, G., P. Molnar, and B. C. Burchfield (1983), Seismicity, fault plane solutions, depth of faulting, and active tectonics of the Andes of Perú, Ecuador and southern Colombia, *J. Geophys. Res.*, *88*, 10,403–10,428, doi:10.1029/JB088iB12p10403.

Tassara, A. (2005), Interaction between the Nazca and South American plates and formation of the Altiplano-Puna plateau: Review of a flexural analysis along the Andean margin (15°-34°S), *Tectonophysics*, *399*, 39–57.

Tassara, A., C. Swain, R. Hackney, and J. Kirby (2007), Elastic thickness structure of South America estimated using wavelets and satellite-derived gravity data, *Earth Planet. Sci. Lett.*, *253*, 17–36, doi:10.1016/j.epsl.2006.10.008.

Tibaldi, A., C. Corazzato, and A. Rovida (2009), Miocene-Quaternary structural evolution of the Uyuni-Atacama region, Andes of Chile and Bolivia, *Tectonophysics*, *471*, 114–135, doi:10.1016/j.tecto.2008.09.011.

Zalohar, J., and M. Vrabec (2007), Paleostress analysis of heterogeneous fault-slip data: the Gauss method, *J. Struct. Geol.*, *29*, 1798–1810.

Zoback, M. L., and M. Magge (1991), Stress magnitudes in the crust, *Philos. Trans. R. Soc. London A*, *337*, 181–194.